PERFORMANCE DEGRADATION OF 100 Gb/s PM-QPSK AND 400 Gb/s

PM-16QAM COHERENT COMMUNICATION SYSTEMS DUE TO

OPTICAL FILTER CASCADE AND CHROMATIC DISPERSION

by

Rami Yousef Al-Dalky

A Thesis Presented to the Faculty of the

American University of Sharjah

College of Engineering

in Partial Fulfillment

of the Requirements

for the Degree of

Master of Science in

Computer Engineering

Sharjah, United Arab Emirates

January 2013

Approval Signatures

We, the undersigned, approve the Master's Thesis of Rami Yousef Al-Dalky

Thesis Title: Performance Degradation of 100 Gb/s PM-QPSK and 400 Gb/s PM-16QAM Coherent Communication Systems Due to Optical Filter Cascade and Chromatic Dispersion

Signature   **Date of Signature**

_____   _____
Dr. Taha Landolsi
Associate Professor, Department of Computer Science and Engineering
Thesis Advisor

_____   _____
Dr. Aly Elrefaie
Visiting Professor, Department of Electrical Engineering
Thesis Co-Advisor

_____   _____
Dr. Mohamed Hassan
Associate Professor, Department of Electrical Engineering
Thesis Co-Advisor

_____   _____
Dr. Rana Ahmed
Associate Professor, Department of Computer Science and Engineering
Thesis Committee Member

_____   _____
Dr. Hasan S. Mir
Assistant Professor, Department of Electrical Engineering
Thesis Committee Member

_____   _____
Dr. Assim Sagahyroon
Professor, Department Head
Department of Computer Science and Engineering

_____   _____
Dr. Hany El-Kadi
Associate Dean
College of Engineering

_____   _____
Dr. Yousef Al-Assaf
Dean
College of Engineering

_____   _____
Dr. Khaled Assaleh
Director of Graduate Studies

Acknowledgment

Foremost, I would like to thank Allah for the perseverance and ambition that he has been bestowed upon me during my master's research and for blessing me throughout my life.

Further, I would like to thank my advisors Dr. Taha Landolsi, Dr. Aly Elrefaie and Dr. Mohamed Hassan for their guidance and invaluable suggestions at every step throughout the thesis. Also I would like to thank them for sharing their knowledge and being patient with me.

Finally, I owe my greatest debt to my family. I would like to thank my parents, my brothers and my sisters for their endless support, love and prayer, and for reminding me every day that impossible is nothing; do your best and Allah will be with you.

To my lovely parents, brothers and sisters

for their endless love and support

Abstract

In the near future, data rates of 100 Gb/s and 400 Gb/s will be used to match the increase in bandwidth demand for capacity. Wavelength division multiplexing (WDM) systems transmit multiple wavelengths simultaneously at high data rates over long distances where the signal passes through multiple optical add drop multiplexers (OADMs) along the fiber link towards the destination. The transmitted signals suffer from dispersion induced from the fiber and OADMs, where these effects are an important limiting factor. The success of high-bit rate, long-haul, point-to-point optical transmission networks depends on the management of the fiber's linear and non-linear effects. In this thesis, we propose to study the impact of cascaded filters as the signals pass through multiple OADMs to determine its effect on the next generation network's data rates. We aim to study the impact of cascaded filters on single-carrier and dual-carrier 100 and 400 Gb/s optical transmission systems. The eye closure penalty (ECP) will be used as a performance evaluation metric. The results indicate that the filter cascade has a severe impact on the performance of dual-carrier systems relative to the case of single-carrier systems. Secondly, chromatic dispersion (CD) effect will be mitigated electronically for 100 and 400 Gb/s systems using fiber-dispersion finite impulse response (FD-FIR) filter. The compensating FIR filter's coefficient will be computed from the impulse response of the inverse of the fiber's transfer function. Bit error rate (BER) versus optical signal-to-noise ratio (OSNR) curve will be used to evaluate the compensating technique. The results indicate that for 100 Gb/s PM-QPSK systems, using 2 samples/symbol with maximum number of taps is the best approach to compensate for CD. While for 400 Gb/s PM-16QAM systems, using 4 samples/symbol with 50% of the maximum number of taps is the best approach to compensate for CD.

Table of Contents

List of Figures

List of Tables

Abbreviations

ADC : Analog-to-Digital Converter

AWG : Array Waveguide-Grating

BER : Bit Error Rate

BPSK : Binary Phase Shift Keying

CD : Chromatic Dispersion

CMA : Constant Modulus Algorithm

CW : Continuous Wave

DCF : Dispersion-Compensating Fiber

DSP : Digital Signal Processing

ECP : Eye Closure Penalty

EDC : Electronic Dispersion Compensation

EDFA : Erbium Doped Fiber Amplifier

FBG : Fiber Bragg Grating filter

FDE : Frequency Domain Equalizer

FD-FIR : Fiber Dispersion-Finite Impulse Response

FSK : Frequency Shift Keying

IMDD : Intensity Modulation Direct Detection

IIR : Infinite Impulse Response

LMS : Least Mean Square algorithm

LO : Local Oscillator

MC : Monte Carlo

MLSE : Maximum Likelihood Sequence Estimation

MMF : Multimode Fiber

MZM : Mach Zehnder Modulation

NLMS : Normalized Least Mean Square

OOK : On-Off Keying

OSNR : Optical Signal-to-Noise Ratio

OXC : Optical Cross Connect

PBC : Polarization Beam Combiner

PBS : Polarization Beam Splitter

PD : Photodiode

PM : Polarization Multiplexing

PMD : Polarization Mode Dispersion

QAM : Quadrature Amplitude Modulation

QPSK : Quadrature Phase Shift Keying

OADM : Optical Add Drop Multiplexer

SMF : Single Mode Fiber

TFF : Thin-Film Filter

WDM : Wavelength Division Multiplexing

WSS : Wavelength Selective Switch

Chapter 1

Introduction

1.1 Purpose of Research

Optical fiber communication systems have been developed rapidly in the last two decades, so the channel data rates of 10 Gb/s and 40 Gb/s will be upgraded in the near future to 100 Gb/s with 50 GHz channel spacing and 400 Gb/s with 100 GHz channel spacing to match the increase of traffic demands in recent years.

The performance of these high speed optical transmissions is severely affected by CD, polarization mode dispersion (PMD) and nonlinear effects of the fiber. Also, it may be affected by filter cascading as the transmission signal will pass through multiple optical add drop multiplexers (OADMs) until it drops to its destination. Addressing these factors' effect on a such high data rates and trying to mitigate these dispersions to achieve the purpose of using these high data rates are considered interesting fields of research.

In this thesis, we propose to study the effect of cascading multiple optical filters on single-carrier/dual-carrier 100 Gb/s polarization-multiplexed quadrature phase shift keying (PM-QPSK) systems using 50 GHz channel spacing. Also, we propose to study the effect of cascading multiple optical filters on single-carrier/dual-carrier 400 Gb/s polarization-multiplexed 16-ary quadrature amplitude modulation (PM-16QAM) systems using 100 GHz and 150 GHz channel spacing. We consider two types of filters: fiber Bragg grating (FBG) and thin-film filter (TFF), where eye closure penalty (ECP)

will be used as a performance evaluation metric.

In addition, we aim to compensate only for CD and assume there is no PMD or fiber non-linear effects. Since the CD is a linear operation on the electrical field, its effect can be undone by linear filtering. We will compensate for a specific amount of CD using FD-FIR filter for 100 Gb/s PM-QPSK and 400 Gb/s PM-16QAM systems using 2 and 4 samples/symbol. The compensating FD-FIR filter's coefficient will be computed from the impulse response of the inverse of the fiber's transfer function after a time window truncation using Nyquist frequency. A bit error rate (BER) versus optical signal-to-noise ratio (OSNR) curve will be used to evaluate the compensating technique.

1.2   Historical Background

Optical fiber communication system is the most preferable technology to transmit data for long distances because of its high speed transmission and high bandwidth.

The research of these systems started in 1970s, where the development of these systems is divided into different generations that increased the transmission capacity of these transmission systems.

The first generation was developed in 1970s, where it used multimode fiber (MMF) at 850 nm. The first generation was severely affected by high attenuation which was about 20 dB/km, CD and modal dispersion which were considered a major limitation for the transmission speed of this system (it was only 45 Mbit/s), and the distance between the repeaters (up to 10 km distance [1]).

The second generation was developed in 1980s and provided a solution for CD by transmitting at 1300 nm. In addition, making the transmission at this wavelength decreased the attenuation to 0.5 dB/km but these systems suffered from modal dispersion because of the use of MMF. This problem was solved with the advent of single mode fiber (SMF) that allowed the system to achieve a bit rate of 1.7 Gb/s with a distance of 50 km between repeaters [2] while the bit rate of MMF was 100 Mb/s.

The third generation was developed at the end of 1980s, by operating at 1550 nm. This made an enhancement by minimizing the attenuation to 0.2 dB/km. The CD

problem was solved by using dispersion-compensating fibers (DCFs). This generation achieved a bit rate of 2.5 Gb/s with a distance of 100 km between repeaters [3].

The forth generation was developed in the last 20 years, where optical amplification using erbium doped fiber amplifiers (EDFA) was used to reduce the number of repeaters. The fourth generation also used wavelength division multiplexing (WDM) to increase the fiber capacity. The development of EDFA and WDM increased the channel data rate from 2.5 Gb/s to 10 Gb/s and 40 Gb/s which are the most likely used channel data rates.

All of these generations used an intensity modulation direct detection (IMDD) receiver that was based on using the intensity modulation of a laser (either direct modulation or external modulation) and the intensity of the transmitted signal. Next it would directly detect the received signal using photodiode (PD). The widely used external modulation is $LiNbO_3$ a Mach-Zehnder modulator (MZM).

Because of the sensitivity of the receiver, coherent optical transmission systems were investigated in 1980s and have the following properties [4] :

- The shot-noise limited receiver sensitivity can be achieved with a sufficient local oscillator (LO) power.

- The ability of phase detection can improve the receiver sensitivity.

These properties allowed an increase in the distance between the repeaters and allowed the use of multilevel modulation schemes to increase the capacity. However, the advent of EDFA and WDM delayed the development of coherent systems for around 20 years, since EDFA increased the distance needed between repeaters and WDM allowed the increase in the capacity of transmission link.

In 2005, coherent transmission techniques became attracted again because of two reasons:

- Multilevel modulation schemes such as m-ary phase shift keying (PSK) and quadrature amplitude modulation (QAM) were implemented by employing the digital coherent receivers.

- High-speed digital signal processing (DSP), that made the retrieval of the complex amplitude of the optical carrier possible from a homodyne-detection receiver.

The development of coherent receivers introduces the use of multilevel modulations which allow transmission at high data rates (e.g, 100 Gb/s with 50 GHz channel spacing and 400 Gb/s with 100 Gb/s channel spacing). In addition, they allow the implementation of digital coherent receivers that offer the possibility for carrier and complex amplitude recovery.

1.3   Structure of the Thesis

This thesis is outlined as follows. In Chapter 2, we provide an introduction and general concepts for some terms needed in the thesis. In Chapter 3, we study the impact of filter cascade on 100 and 400 Gb/s optical communication systems. Section. 3.1 provides some information about the concept of filter cascade and optical filter technologies. Section. 3.2 provides a description of related works in filter cascade and introduces our work. Section. 3.3 presents the system model of single-carrier 100 and 400 Gb/s systems used in simulation and their results. Finally, Section. 3.4 presents the system model of dual-carrier 100 and 400 Gb/s systems used in simulation and their results.

In Chapter 4, we compensate for chromatic dispersion (CD) using a fiber-dispersion finite impulse response (FD-FIR) filter for 100 and 400 Gb/s systems. Section. 4.1 presents a brief introduction about CD compensating techniques. Section. 4.2 provide a description of related works in CD equalization. Section. 4.3 describes the dispersion compensation filter design by defining the number of taps required to compensate for a specific amount of dispersion. Section. 4.4 describes the system model of 100 and 400 Gb/s systems used in simulation. Section.4.5 presents the simulation results for 100 and 400 Gb/s using 2 and 4 samples/symbol for each system. Finally, Section. 4.6 computes the maximum tolerable fiber distance for a CD compensating filter for 100 and 400 Gb/s systems.

Conclusions are summarized in Chapter 5 along with suggestions for future research.

Chapter 2

General Concepts

In this chapter, we will review some general concepts about coherent detection and some factors that are considered as limitation factors for the high speed optical fiber transmission. Also, we will discuss some of the dispersion compensation techniques that may be used to mitigate the effects of these factors.

2.1   Overview of Coherent Detection

The main idea behind coherent detection is the mixing of the incoming signal with LO that allows the receiver to obtain the amplitude and phase of the incoming signal. The mixing of the optical signal and the LO is done with a 90° hybrid mixer in front of the PDs.

Fig. 2.1 shows the configuration of the coherent optical receiver. The incoming optical signal is expressed as [5]:

$$E_s(t) = I(t)\cos(\omega_s t + \phi_n) - Q(t)\sin(\omega_s t + \phi_n) \tag{2.1}$$

Where $I(t)$ is the in-phase of the incoming signal, $Q(t)$ is the quadrature-phase of the incoming signal, ω_s is the angular frequency. ϕ_n is the phase noise.

The optical field of LO at the receiver is given by:

$$E_{LO}(t) = A_{LO}(t)\cos(\omega_{LO}t + \phi_{LO}) \tag{2.2}$$
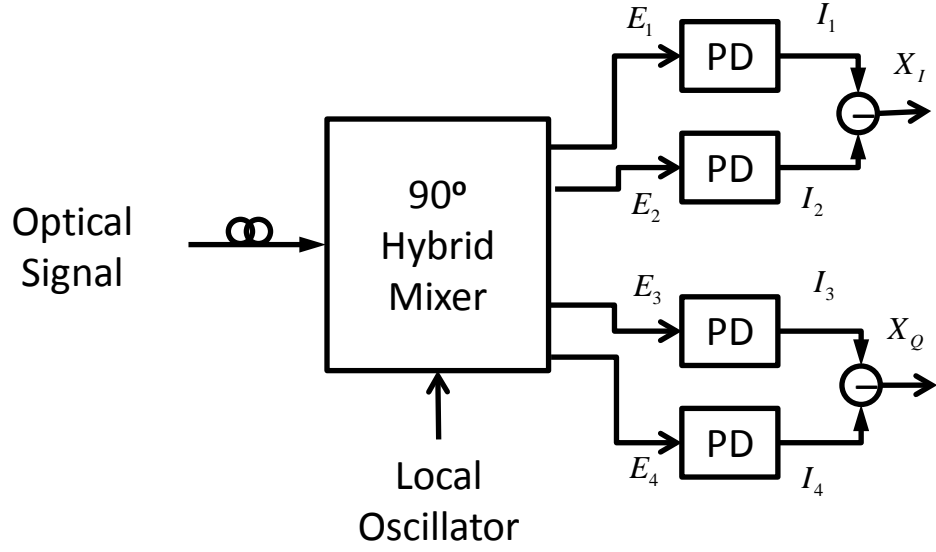
Figure 2.1: Schematic diagram for coherent receiver.

Where $A_{LO}(t)$ is complex amplitude of the LO, ω_s is the angular frequency and ϕ_{LO} is the phase noise of the LO.

In a homodyne receiver, $\omega_s = \omega_{LO}$ and the phase noise angles are equal through the phase lock loop. From the 90° hybrid mixer we can obtain four outputs as below:

$$E_1 = \frac{1}{L}(I(t)\cos\omega_s t - Q(t)\sin\omega_s t + A_{LO}(t)\cos\omega_{LO}t) \tag{2.3}$$

$$E_2 = \frac{1}{L}(I(t)\cos\omega_s t - Q(t)\sin\omega_s t - A_{LO}(t)\cos\omega_{LO}t) \tag{2.4}$$

$$E_3 = \frac{1}{L}(I(t)\cos\omega_s t - Q(t)\sin\omega_s t + A_{LO}(t)\sin\omega_{LO}t) \tag{2.5}$$

$$E_4 = \frac{1}{L}(I(t)\cos\omega_s t - Q(t)\sin\omega_s t - A_{LO}(t)\sin\omega_{LO}t) \tag{2.6}$$

Where L^2 is the power loss of the 90° hybrid mixer. Here we assume that L = 1.

The outputs of the upper PDs are given by:

$$I_1(t) = \frac{R}{2}\left[(I(t) + A_{LO}(t))^2 + Q^2(t)\right] \tag{2.7}$$

$$= \frac{R}{2}\left[I^2(t) + Q^2(t) + A_{LO}^2(t) + 2I(t)A_{LO}(t)\right] \tag{2.8}$$

$$I_2(t) = \frac{R}{2}\left[(I(t) - A_{LO}(t))^2 + Q^2(t)\right] \tag{2.9}$$

$$= \frac{R}{2}\left[I^2(t) + Q^2(t) + A_{LO}^2(t) - 2I(t)A_{LO}(t)\right] \tag{2.10}$$

Where R is the responsivity of the PDs. The balanced detector outputs of the in-phase and the quadrature-phase are given as:

$$X_I(t) = I_1(t) - I_2(t) \tag{2.11}$$

$$= 2RI(t)A_{LO}(t) \tag{2.12}$$

$$X_Q(t) = I_3(t) - I_4(t) \tag{2.13}$$

$$= 2RQ(t)A_{LO}(t) \tag{2.14}$$

It is clear that $X_I(t)$ and $X_Q(t)$ are proportional to I(t) and Q(t), respectively.

2.2 Chromatic Dispersion

CD is a phenomenon that occurs in SMF, because the phase velocity of a wave depends on its frequency (group velocity delay become a function of wavelength).

It has two main dispersion types:

1. Material Dispersion

   It occurs because the refraction index $n(\lambda)$ of a fiber is a function of wavelength. This frequency-dependent dispersion causes the different spectral components

23
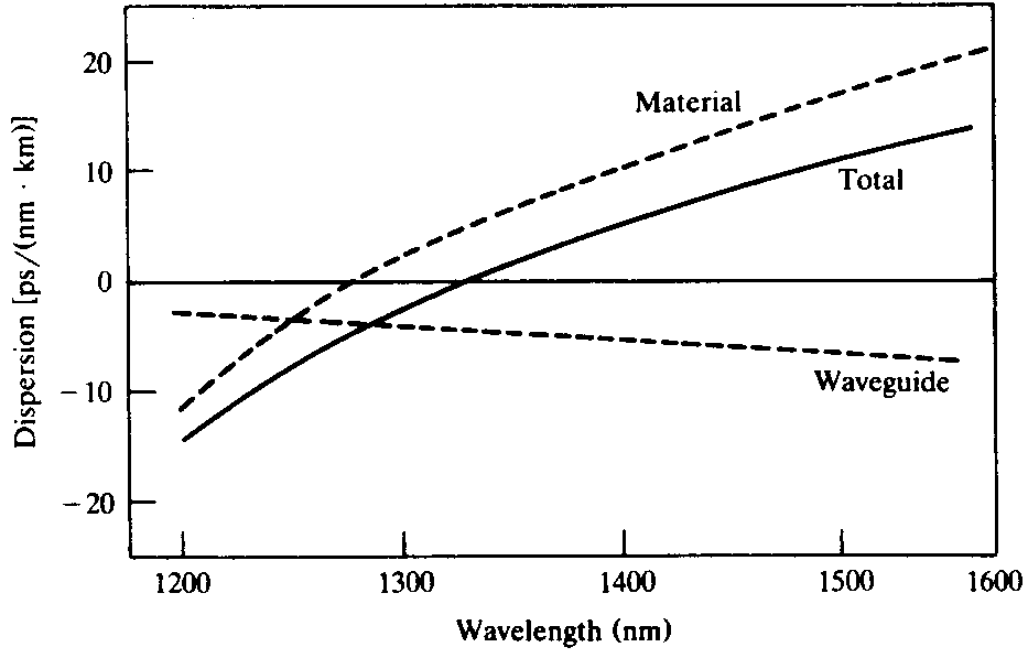
Figure 2.2: Magnitude of material and waveguide dispersion of SMF after ref.[7].

that are sent at the same time to arrive at the receiver at different times.

2. Waveguide Dispersion

This happens because the power distribution of a mode between the core and cladding of the fiber is a function of the wavelength.

In general, for a waveguide mode with an angular frequency $\omega(\beta)$ with a propagation constant β, the electromagnetic fields in the propagation direction z oscillate proportional to e(βz - ωt).

CD is the resultant dispersion of material and waveguide that is measured in $ps/nm.km$ which is shown in Fig. 2.2 and is given by the equation:

$$D = \frac{1}{L}\frac{d\tau}{d\lambda} \quad , \quad \frac{d\tau}{d\lambda} = \frac{d\tau}{d\omega}\frac{d\omega}{d\lambda} \tag{2.15}$$

Where τ is the group delay and L is the fiber length. $\omega = 2\pi f$, where f is the central frequency corresponding to the wavelength $\lambda = 1.553\mu m$.

24

2.3 Polarization Mode Dispersion

PMD arises from the fact that fibers are not perfectly circularly symmetric where there exists a small level of birefringence. This causes a different arrival time of the different polarization components of an input light pulse that is transmitted by the optical fiber. The light pulse can always be decomposed into pairs of orthogonal polarization modes. These polarization modes propagate at different speeds according to a slow and fast axis induced by the birefringence of the fiber. Fig. 2.3 shows the polarization mode dispersion phenomenon.

The effect of PMD is not considered in this thesis, but several papers have been published and it is a topic for future research.
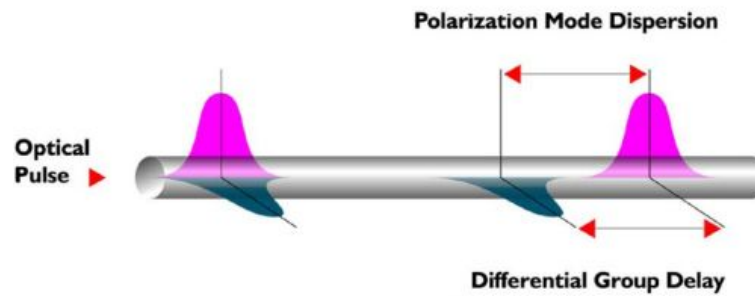
Figure 2.3: Schematic of polarization mode dispersion of SMF after ref.[8].

2.4 Dispersion Compensation Techniques

There are many mitigation techniques that are used for CD compensation, such as:

- Dispersion-Compensating Fiber (DCF)

  DCF has been developed to compensate for CD in the 1550 nm wavelength range. DCF is a spool of special fiber several kilometers long that provides a large negative CD, placed after specific distance of transmission (usually 80 km) so that the total dispersion of the two fibers in series is zero. However, DCF introduces additional loss, therefore requiring additional optical amplifiers that increase noise

and cost of the system. Fig. 2.4 shows DCF placed on a fiber between a transmitter and a receiver.
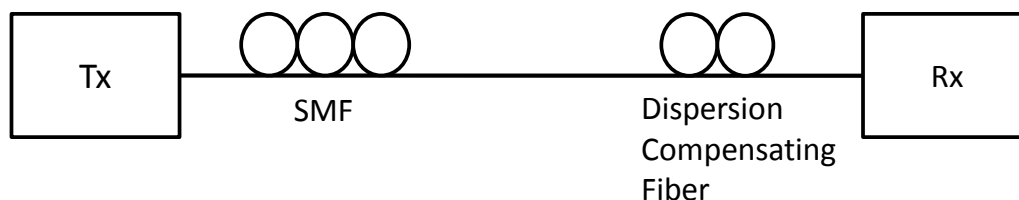
Figure 2.4: Dispersion compensating fiber placed between transmitter and receiver.

This type of compensation is used with on-off keying (OOK), while it is not needed with homodyne receivers where CD is equalized using electronic dispersion compensation (EDC).

- Electronic Dispersion Compensation

  EDC techniques are only possible for homodyne receiver, where there are multiple techniques that can be used to compensate for CD such as:

  - Fiber dispersion finite impulse response (FD-FIR) filter.

  - Infinite impulse response (IIR) filter.

  - FIR based least mean square (LMS) filter.

  - FIR based constant modulus algorithm (CMA) filter.

  - Frequency domain equalizer (FDE).

In this thesis, we are only studying dispersion compensation of CD using a FD-FIR filter.

For PMD, three major mitigation techniques are used [10]:

- Optical Compensation.

- Opto-Electronic Compensation.

- Electronic Compensation.

26

2.5   Finite Impulse Response Filter

FIR filter is a digital filter that has an impulse response that reaches zero in a finite number of samples. Fig. 2.5 below shows the structure of FIR filter of order N-1, where it has N taps and N-1 delay units. The operation of FIR filter is described by the following equation, which defines the output sequence y[n] in terms of its input sequence x[n]:

$$y[n] = \sum_{i=0}^{N-1} b_i x[n-i]$$
(2.16)

If the signal x[n] is replaced by an impulse $\delta[n]$ then:

$$h[n] = \sum_{i=0}^{N-1} b_i \delta[n-i] = b_n, \text{ with n = 0 to N-1}$$
(2.17)
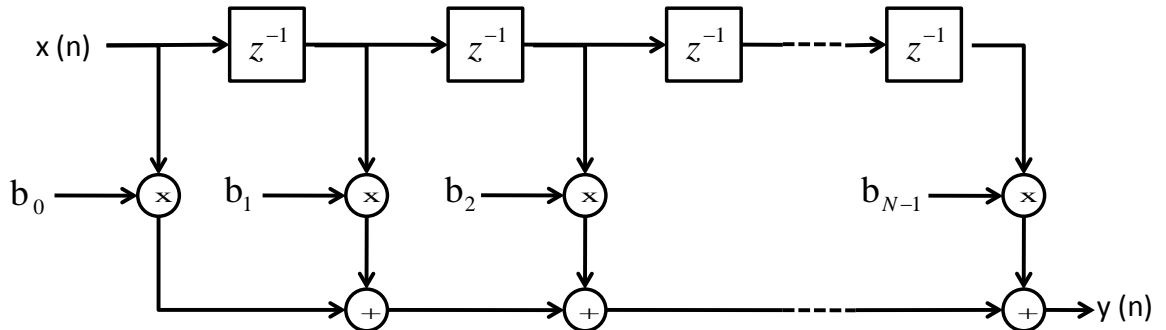
Figure 2.5: Schematic of FIR filter of order N-1.

Chapter 3

Impact of Cascaded Optical Filters On 100 Gb/s PM-QPSK and 400 Gb/s PM-16QAM Coherent Communication Systems

3.1 Introduction

In the near future, data rates of 100 Gb/s and 400 Gb/s will be used to match the increase in bandwidth demand. Optical networks use WDM systems to transmit multiple wavelengths simultaneously at high data rates over long distances. As shown in Fig. 3.1, optical channels typically pass through several switching nodes (e.g, optical cross-connects (OXCs), OADMs) before reaching their destinations. Each OADM typically comprises two filters, where the amplitude and dispersion characteristics of these filters may cause a distortion of the transmitted signal. There is a variety of optical filter technologies that can be used in the multiplexer/demultiplexer inside an OADMs [12], [19], [24] such as:

- Array waveguide grating (AWG).

- Thin film filter (TFF).

- Fiber Bragg grating (FBG).

- Liquid crystal.
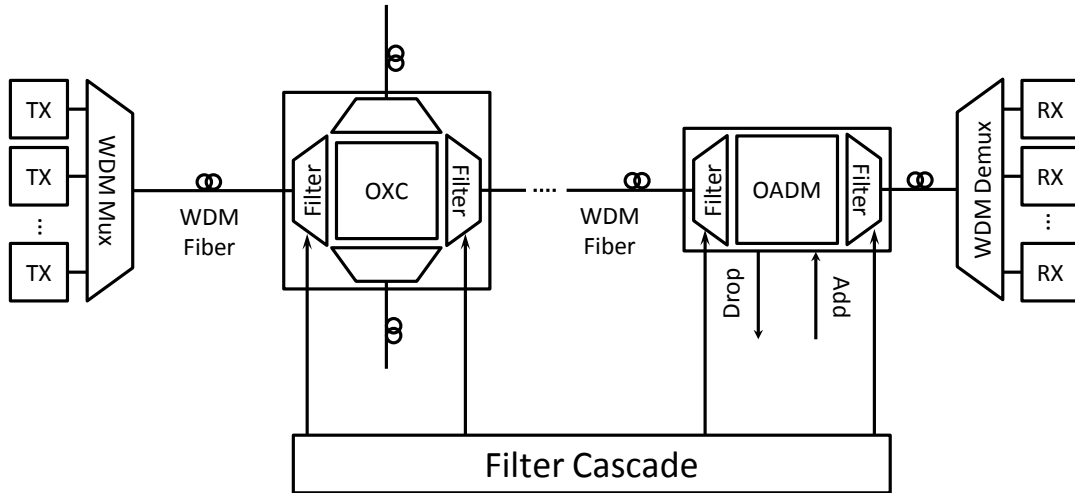
Figure 3.1: Scheme of filter cascading in an optical transmission system

AWG could be used in OADMs since it has no dispersion but it has a high insertion loss which can be higher than 7dB [12]. Liquid crystal can be used in OADMs because of its low power consumption and low loss, but it is considered not stable to be used in OADMs as it is required to operate under specific environmental conditions [15], [16].

FBG and TFF are attractive to be used in the multiplexer/demultiplexer inside OADMs. FBG could be used in OADMs because of its low insertion loss and flat passband, also it has a low manufacturing cost. However, FBG has higher dispersion characteristics compared to TFF.

TFF was adopted very early on and has been widely used for multiplexer/demultiplexer in OADMs [17]-[19] because of its characteristics (stable, low insertion loss, flat passband and low dispersion characteristics) [20]. This made TFF the best choice to be used in OADMs.

3.2 Related Works

Performance degradation of optical communication systems employing different modulation schemes due to filter cascade has been investigated in [21]-[31].

The impact of cascading filters on the magnitude and the phase characteristics of the (de)multiplexer transfer function have been investigated since they are considered

an important factors in determining the distortion-induced penalties. The ECP due to filter cascade for 2.5, 10 and 40 Gb/s systems has been studied in [21]-[23],[27] using TFF.

The power penalty at the receiver has been computed in [24]-[26] due to the accumulated dispersion of optical filter cascades in WDM optical networks.
Using flat-top FBG and TFF filters, it has been noticed that the dispersion rather than filter amplitude effects dominate the cascade power penalty, which increases with the dispersion slope as the signal frequency is detuned from the cascade zero-dispersion point.

The impact of a liquid-crystal based wavelength selective switch (WSS) cascade on the end-to-end performance of 127 Gb/s PM-QPSK systems at 50 GHz spacing has been investigated experimentally and through simulations in [28].

A system of 224 Gb/s PM-16QAM was generated with 50 GHz channel spacing and the wavelengths were passed through three WSSs without any contribution of measurable filtering or crosstalk penalty [29].

The transmission of dual-carrier 115.2 Gb/s DP-QPSK with 50 GHz channel spacing has been characterized in [30] and the wavelengths were passed through 10 microelectromechanical system (MEMs)-mirror-based WSSs.

The compatibility of 448 Gb/s dual-carrier PM-16QAM modulation with a 87.5 GHz channel spacing in the presence of cascaded optical filtering has been experimentally verified in [31]. The results show that 448-Gb/s dual-carrier PM-16QAM on an 87.5 GHz channel spacing is a suitable candidate for next-generation meshed networks.

In this chapter, we propose to study the effect of cascading multiple optical filters on single-carrier 100 Gb/s PM-QPSK systems using 50 GHz channel spacing. Also, we propose to study the effect of cascading multiple optical filters on single-carrier 400 Gb/s PM-16QAM systems using 100 GHz and 150 GHz channel spacing.

Since the use of single-carrier 100 and 400 Gb/s is considered a challenge because the use of low speed electronics, some researches have showed interest in dual-carrier transmission. In dual-carrier, the symbol rate is shared between two carriers where each

carrier carries the half of the transmitted data.

This means that, for a 100 Gb/s PM-QPSK dual-carrier system, the optical and electrical components need to operate at 12.5 GSymbol/s (which already exists) instead of 25 GSymbol/s in the case of single-carrier .In contrast, for a 400 Gb/s PM-16QAM dual-carrier system, the optical and electrical components need to operate at 25 GSymbol/s (which is already used to develop single-carrier 100 Gb/s PMQPSK products) instead of 50 GSymbol/s in the case of single carrier.

Because of this, we also aim to study the effect of cascading multiple optical filters on dual-carrier 100 Gb/s PM-QPSK systems using 50 GHz channel spacing and dual-carrier 400 Gb/s PM-16QAM systems using 100 GHz and 150 GHz channel spacing.

ECP is used as a performance evaluation metric, which is defined as: $\delta_{EC} = 20log(a/b)$ where a is the eye opening for the ideal eye and b for the distorted one. ECP has been calculated for two types of filters cascade: FBG and TFF, since TFF is the most widely used filter in OADMs. Also, we considered FBG because of its low manufacturing cost and it has been investigated by MIT Lincoln lab [24]-[26].

The amplitude and the dispersion characteristics of FBG filters used in our simulation are similar to the characteristics measured for FBG used in [24],[25]. TFF filters used in our simulation have been modeled as Butterworth filters [23],[27] whose order is adjusted to match the FBG filters amplitude response at the same bandwidth.

3.3   Single Carrier 100 and 400 Gb/s

3.3.1   System Model

To model the end-to-end system, we used VPItransmissionMaker tool [45]. The simulation block diagram is shown in Fig. 3.2. The transmitter that is shown in Fig. 3.3 consists of a continuous wave (CW) laser that is followed by an ideal polarization beam splitter (PBS) to split the laser into X and Y components. Each component is fed into Mach Zehnder Modulator (MZM) to generate a QPSK signal with a symbol rate of 25 GSymbol/s or a 16-QAM signal with a symbol rate of 50 GSymbol/s. An ideal po-

larization beam combiner (PBC) is used to combine the two orthogonal polarizations and couple them into the transmission line. The combined signal will pass through a cascade of multiple filters before reaching the receiver.

In this model, only the *X*-component of the signal passing through the filter cascade will be analyzed. This is because the focus of this study is to simulate the filter cascade impact on the transmitted signal without any consideration of the CD and PMD of a
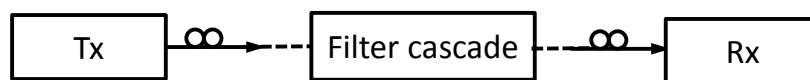
Figure 3.2: Simulation block diagram for single carrier.
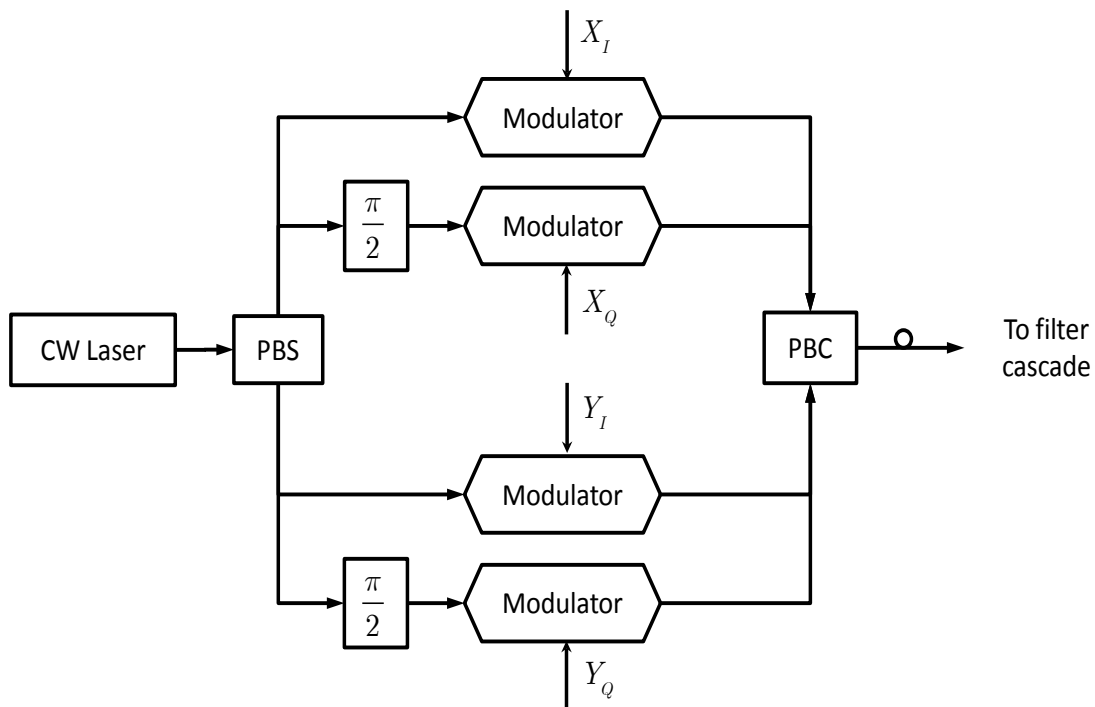
Figure 3.3: Block diagram of the optical transmitter used in the simulation of a single-carrier.

transmission fiber. We consider a homodyne receiver as shown in Fig. 3.4 with an ideal LO synchronized to the X-component. The LO and the received signal are applied to a 90° hybrid mixer, where the in-phase and the quadrature-phase signals of the *X*-component are demodulated using four balanced PDs. The current from the PD is filtered by a third order Butterworth electric filter that has a 3-dB bandwidth of 3/4 the symbol rate.
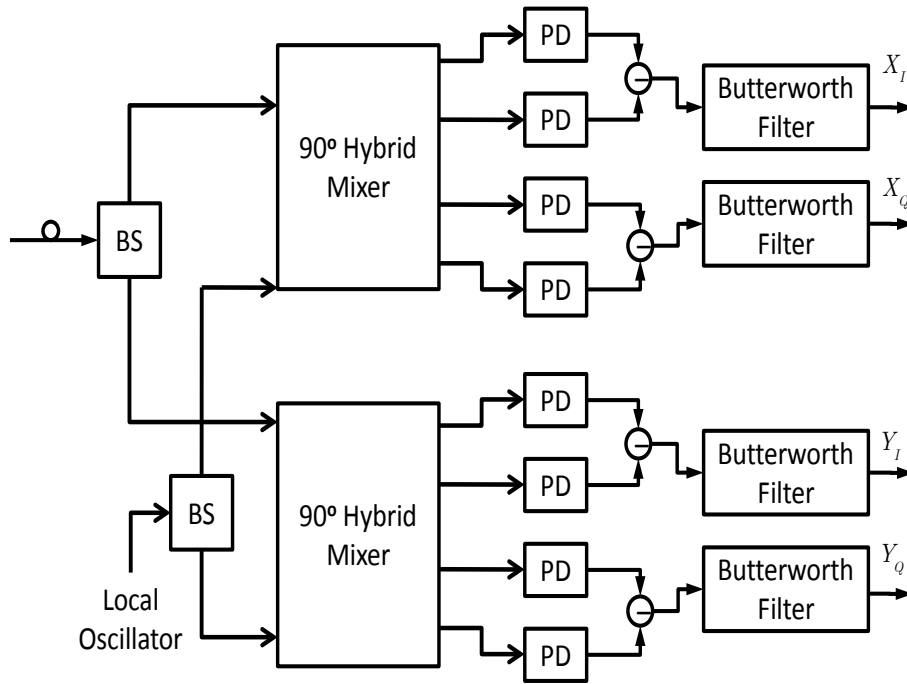
Figure 3.4: Block diagram of the optical homodyne receiver used in the simulation of a single-carrier.

3.3.2   Simulation Results

3.3.2.1   Single-Carrier 100 Gb/s PM-QPSK System

In this section, we use FBG and TFF filters at 50 GHz channel spacing with 3-dB bandwidth of 43 GHz. Fig. 3.5 shows the amplitude response and the dispersion for one FBG and one TFF with 3-dB bandwidth of 43 GHz at 50 GHz channel spacing.

The TFF shown in the figure is a fifth order Butterworth filter, which gives the same amplitude response as the FBG filter used in this section[24],[25]. When cascading
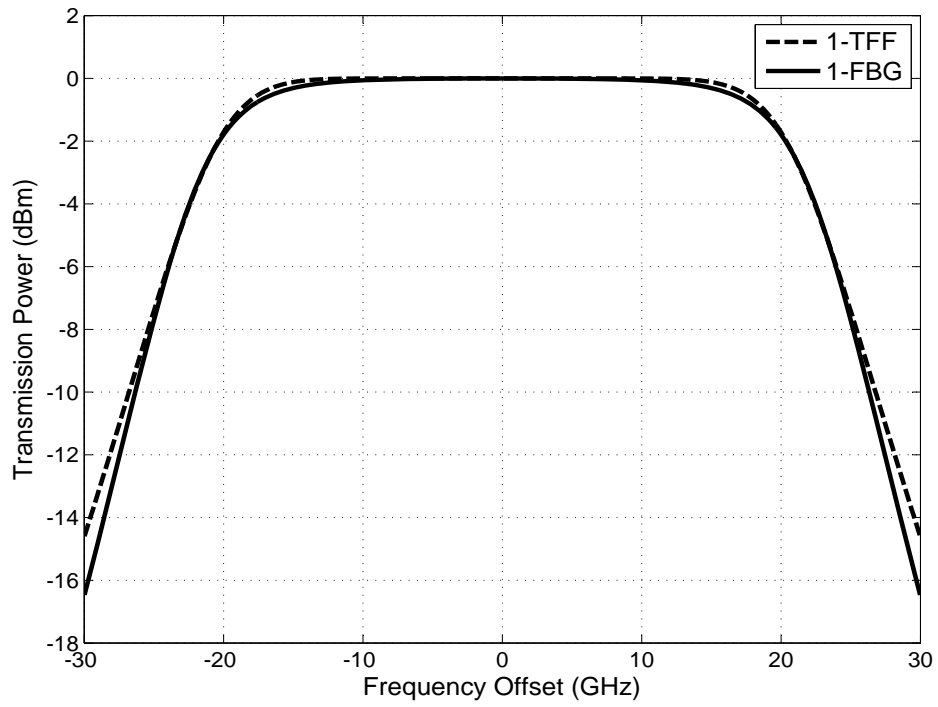
(a)
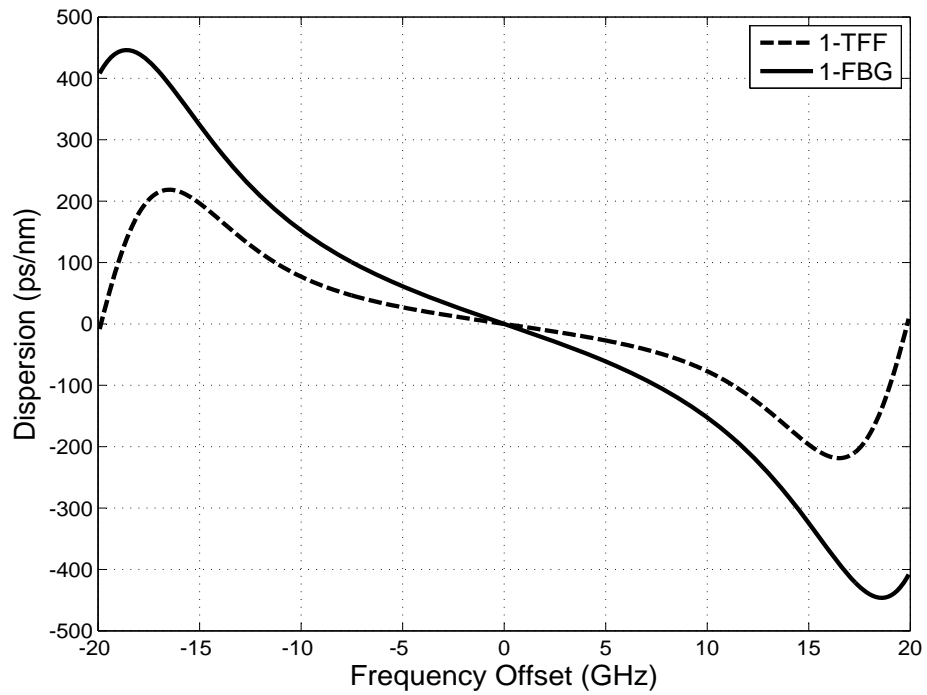
(b)

Figure 3.5: Amplitude (a) and dispersion (b) for one 43 GHz FBG and TFF at 50 GHz channel spacing.

eight FBG and TFF, the resultant bandwidth is about 36 GHz. Also the figure indicates that TFF has lower dispersion than that of the FBG filter.

The simulation has been performed to study the effect of cascading a number of FBG and TFF filters on the in-phase of the X-component of the receiver output. Fig. 3.6 shows the effect of cascading six FBG and TFF filters on the eye diagram. It can be qualitatively shown that the eye opening when cascading six TFF filters is better than the one when cascading six FBG filters.

Fig. 3.7 shows the ECP as a function of the number of FBG and TFF with 3-dB bandwidth of 43 GHz at 50 GHz channel spacing. The results indicate that for 3-dB ECP, we can only cascade 4 TFF and 2 FBG filters with 3-dB bandwidth of 43 GHz. In addition, we can only cascade 10 TFF and 4 FBG filters with 3-dB bandwidth of 43 GHz at 6-dB ECP.

Moreover, we also used FBG and TFF filters with 3-dB bandwidth of 32 GHz at 50 GHz channel spacing with the same amplitude response. In this case, we can only cascade 4 TFF and a single FBG filters while incurring a 3-dB ECP, while we can cascade up to 6 TFF and 2 FBG filters at 6-dB ECP. This can be summarized by Table 3.1.
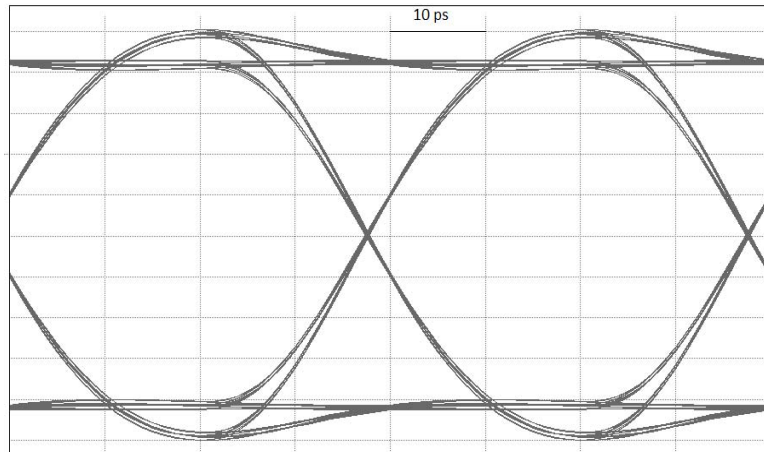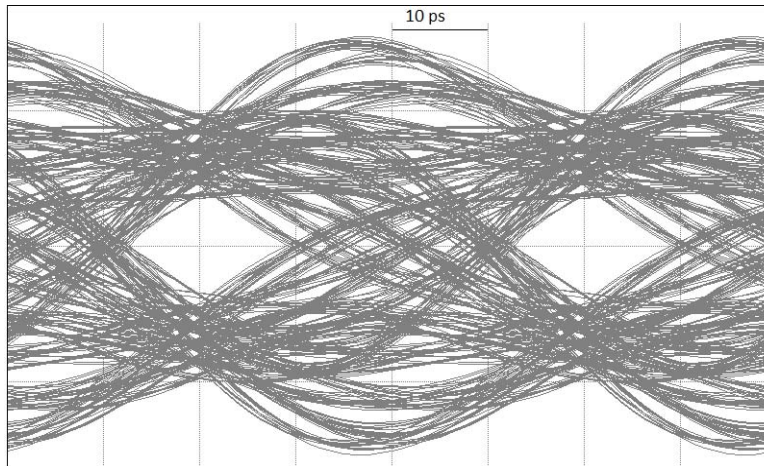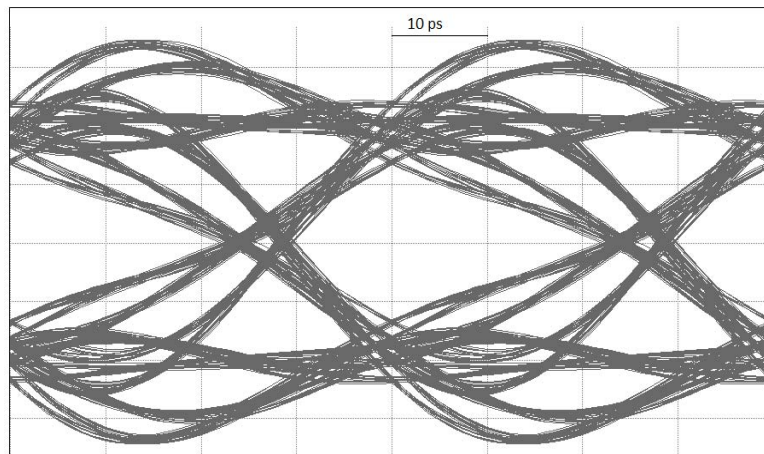
Figure 3.6: Eye diagrams of ideal QPSK (a) and when cascading six 43 GHz FBG (b) and TFF (c) at 50 GHz channel spacing for a single carrier QPSK.

Figure 3.7: Eye closure penalty for 32 GHz and 43 GHz FBG and TFF filters at 50 GHz channel spacing for a single carrier QPSK.

Filter Types	No. of cascaded filters	
	@ 3-dB ECP	@ 6-dB ECP
TFF 43 GHz	4	10
FBG 43 GHZ	2	4
TFF 32 GHz	4	6
FBG 32 GHZ	1	2

Table 3.1: No. of filters at specific ECP for FBG and TFF in a single-carrier system with 50 GHz channel spacing.

3.3.2.2   Single-Carrier 400 Gb/s PM-16QAM System

For the 400 Gb/s system, we studied both 100 and 150 GHz channel spacing. For the first case, we considered FBG and TFF filters with 3-dB bandwidth of 90 GHz at 100 GHz channel spacing. The amplitude response and the dispersion for one FBG and one TFF with 3-dB bandwidth of 90 GHz at 100 GHz channel spacing is shown in Fig. 3.8. The TFF shown in the figure is a sixth order Butterworth filter, which gives the same amplitude response as the FBG used in this section [24],[25]. The resultant bandwidth is around 79 GHz when cascading four FBG and TFF. Moreover, the figure indicates that TFF has lower dispersion than that of the FBG filter.

We aim to study the effect of cascading a number of FBG and TFF filters on the in-phase of the X-component of the receiver output. The effect of cascading two FBG and TFF filters on the eye diagram is shown in Fig. 3.9. It can be clearly shown that the eye opening when cascading two TFF filters is better than the one when cascading two FBG filters.

For the second case, we considered FBG and TFF filters with 3-dB bandwidth of 135 GHz at 150 GHz channel spacing. The amplitude response and the dispersion for one FBG and one TFF with 3-dB bandwidth of 135 GHz at 150 GHz channel spacing is shown in Fig. 3.10. The TFF shown in the figure is a sixth order Butterworth filter, which gives the same amplitude response as the FBG used in this section [24],[25].

The simulation also has been performed to study the effect of cascading a number of FBG and TFF filters on the in-phase of the X-component of the receiver output. Fig. 3.11 shows the effect of cascading four FBG and TFF filters on the eye diagram. It can be qualitatively shown that the eye opening when cascading four TFF filters is better than the one when cascading four FBG filters.

Fig. 3.12 shows the ECP as a function of the number of FBG and TFF with 3-dB bandwidth of 90 GHz at 100 GHz channel spacing. The results indicate that for 6-dB ECP, we can only cascade 4 TFF and a single FBG filters with 3-dB bandwidth of 90 GHz at 100 GHz channel spacing.

In addition, for a 400 Gb/s system at channel spacing of 150 GHz using FBG and
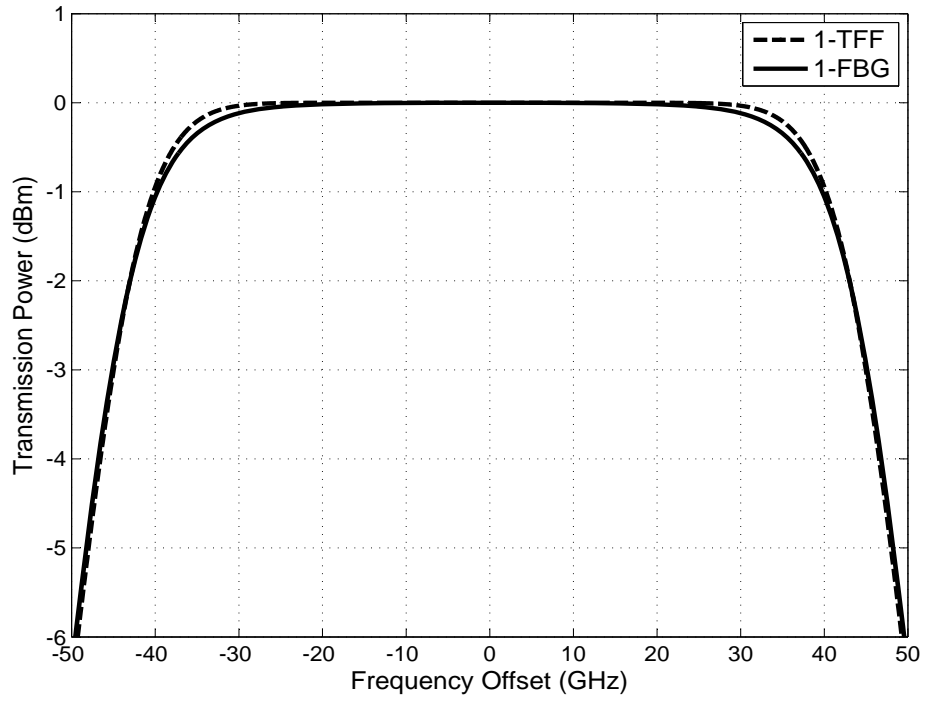
(a)
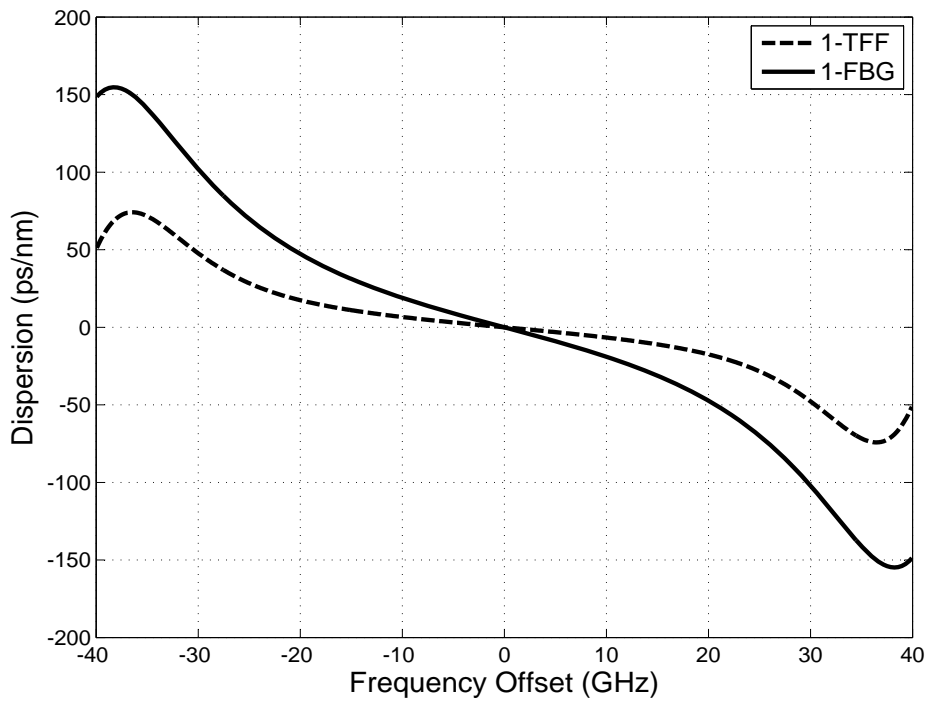
(b)

Figure 3.8: Amplitude (a) and dispersion (b) for one 90 GHz FBG and TFF at 100 GHz channel spacing.
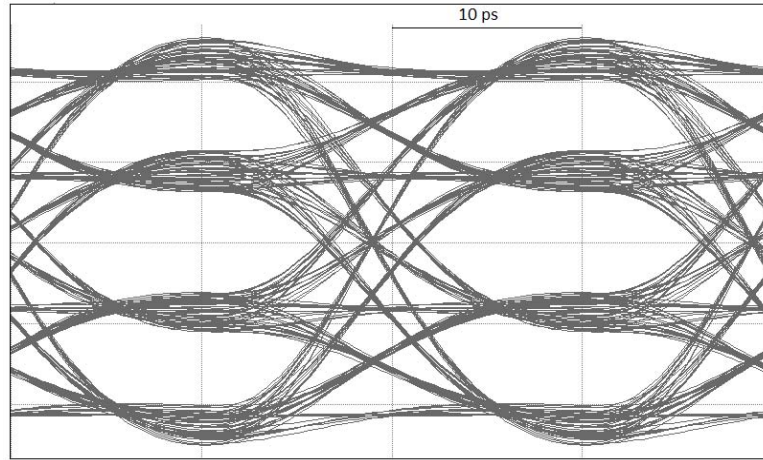
(a)
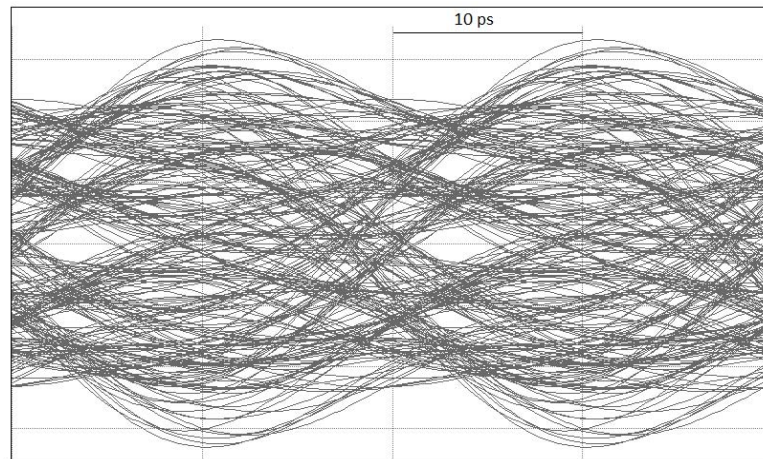
(b)
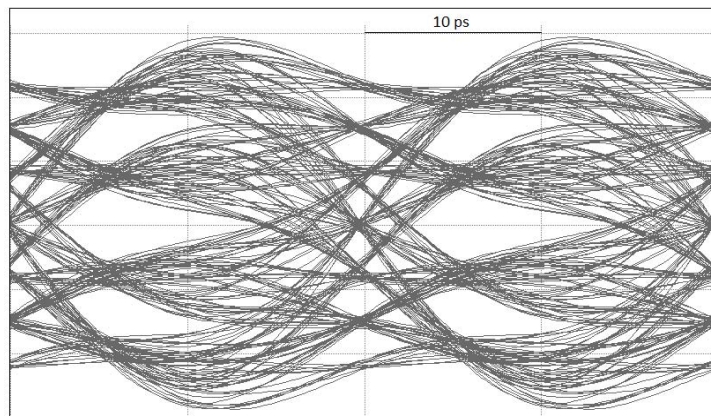
(c)

Figure 3.9: Eye diagrams of ideal 16-QAM (a) and when cascading two 90 GHz FBG
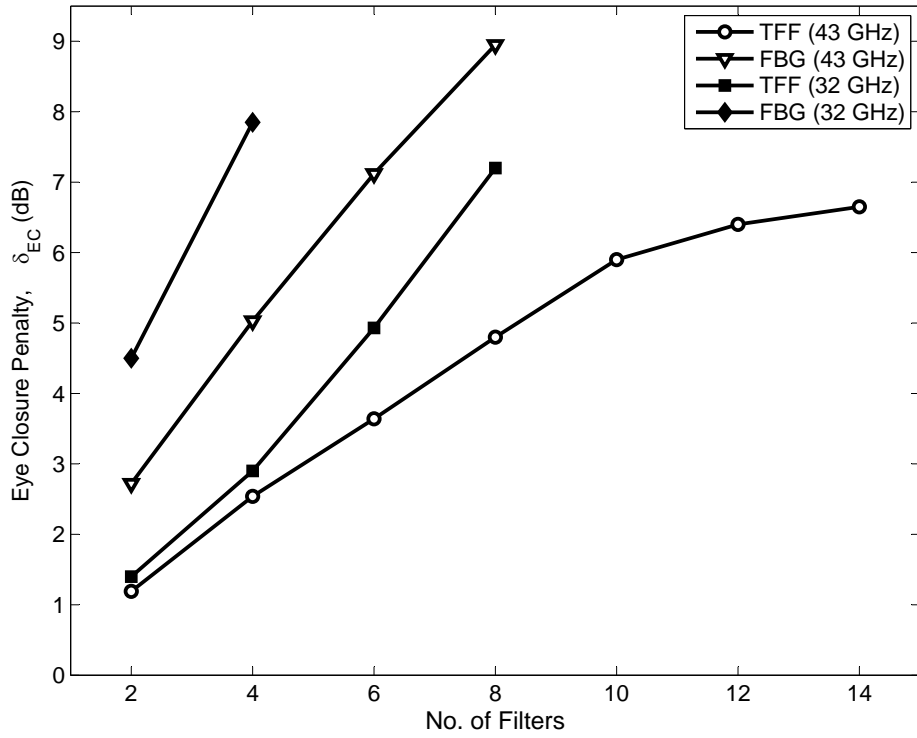(b) and TFF (c) at 100 GHz channel spacing for a single carrier 16-QAM.
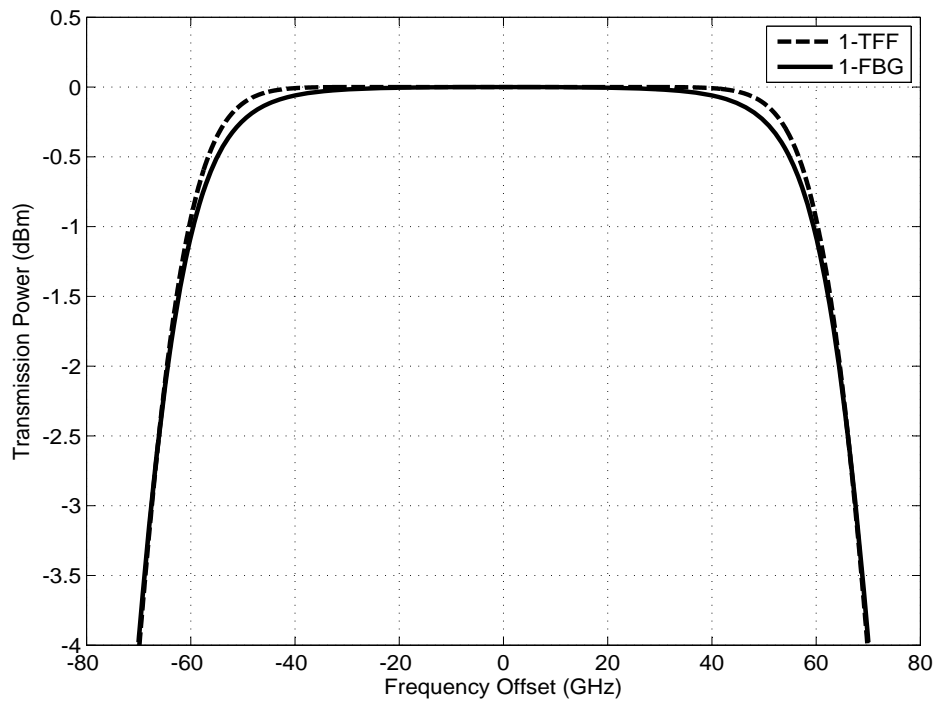
(a)
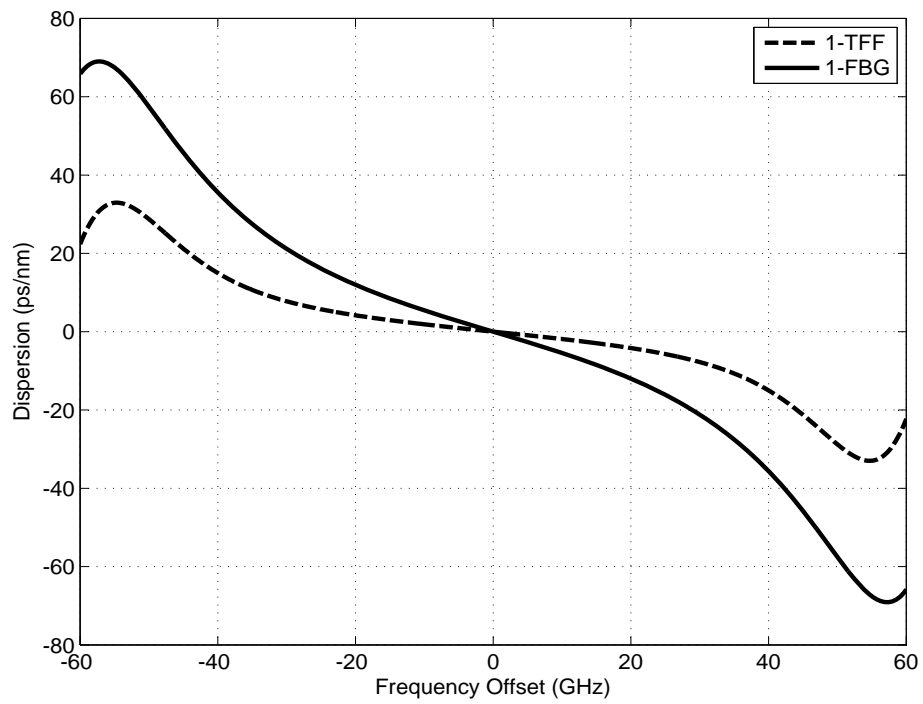
(b)

Figure 3.10: Amplitude (a) and dispersion (b) for one 135 GHz FBG and TFF at 150 GHz channel spacing.
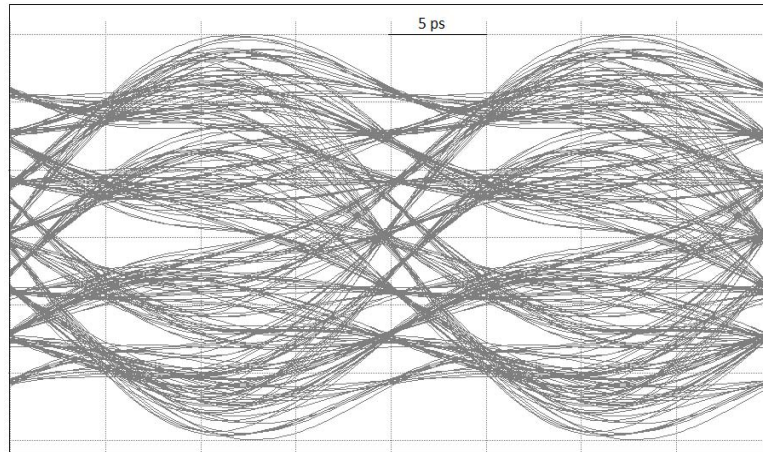
(a)
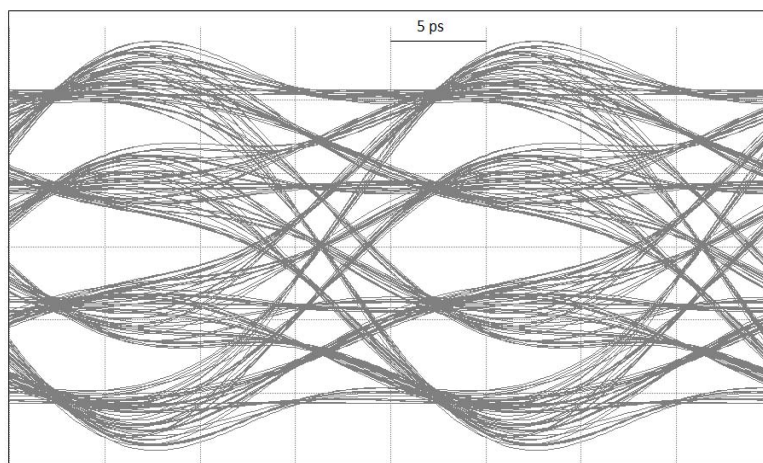
(b)

Figure 3.11: Eye diagrams of cascading four 135 GHz FBG (a) and TFF (b) at 150 GHz channel spacing for a single carrier 16-QAM.

TFF filters with 3-dB bandwidth of 135 GHz, simulation results show that at 3-dB ECP, we can only cascade 10 TFF and 2 FBG filters.
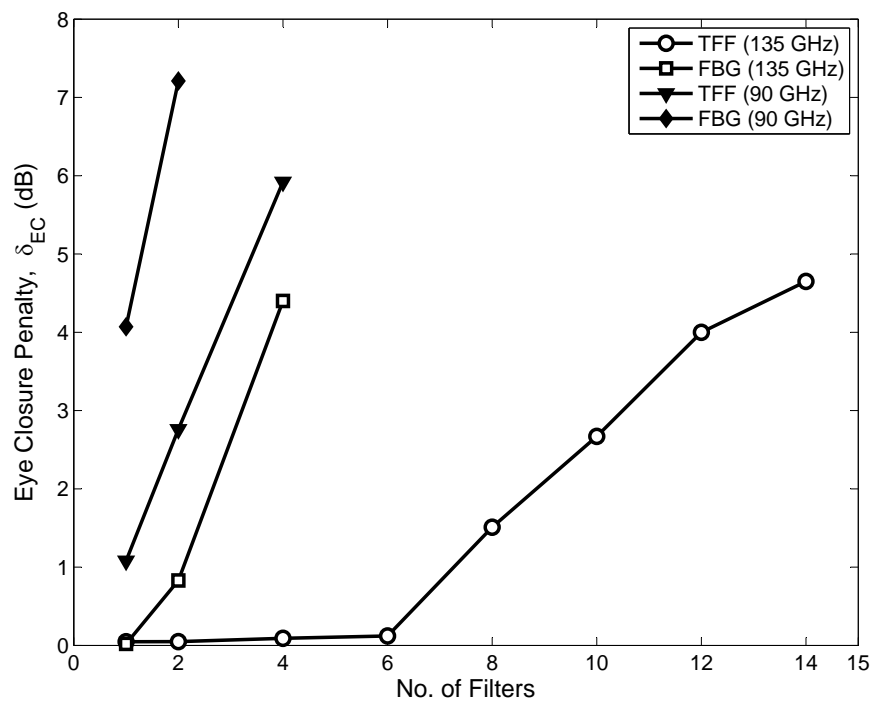
Figure 3.12: Eye closure penalty for 90 GHz and 135 GHz FBG and TFF filters for single carrier 16-QAM.

3.4 Dual Carrier 100 and 400 Gb/s

3.4.1 System Model

The block diagram of a dual-carrier system is shown in Fig. 3.13. From the figure, we can notice that there are two CW lasers, one for each carrier. The two transmitters' carrier frequencies are typically separated by 20 GHz in terms of a 100 Gb/s QPSK system at 50 GHz channel spacing. In terms of a 400 Gb/s 16-QAM system at 100 GHz channel spacing, the two transmitters' carrier frequencies are typically separated by 45 GHz. Each CW laser will be splitted by an ideal PBS into X and Y components.
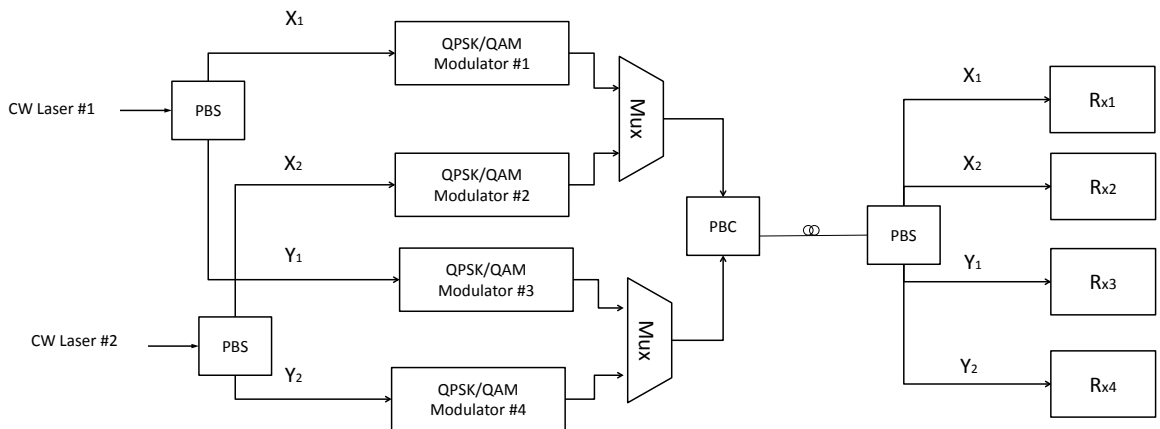
Figure 3.13: Block diagram for a dual carrier system.
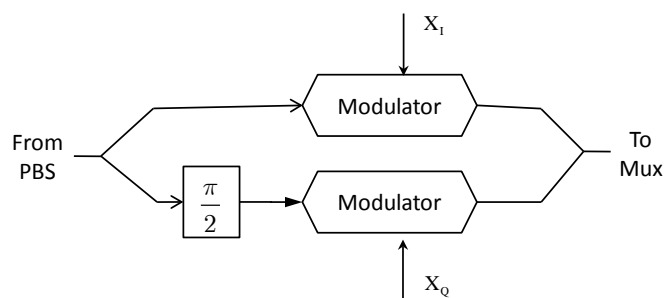
Figure 3.14: Schematic diagram of a QPSK/QAM modulator.

Each component is fed into a QPSK/QAM modulator which is a quadrature MZM that is shown in Fig. 3.14. The MZM generates a QPSK signal for 100 Gb/s with a

44

symbol rate of 12.5 GSymbol/s or a 16-QAM signal for 400 Gb/s with a symbol rate of 25 GSymbol/s. Each component of each carrier is carrying 25 Gb/s in terms of 100 Gb/s PM-QPSK system or 100 Gb/s in terms of 400 Gb/s PM-16QAM system.

The output modulated signal of the X component of the two carriers are combined by ideal mux, which is the same for the Y component. The resultant X and Y components are combined by an ideal PBC into orthogonal polarizations. At the receiver side, PBS is used to split the received signal into X and Y components. The X component is fed into Rx_1 and Rx_2, and the Y component is fed into Rx_3 and Rx_4.

In this thesis, we will only focus on the effect of filter cascade on the transmitted signal, without considering the effects of a transmission fiber. Because of this, we will analyze one of the X-components of the combined transmitted signal.

Fig. 3.15 shows the block diagram of one of the X-components' receiver. We consider a homodyne receiver with an ideal LO that is synchronized to the X-component of one of the two carriers that it designed to receive. The LO and the received signal are applied to a 90° hybrid mixer, where the in-phase and the quadrature-phase signals of the X-component are demodulated using four balanced PDs. We use a third order Butterworth electric filter that has a 3-dB bandwidth of 3/4 the symbol rate to filter the current from the PD.
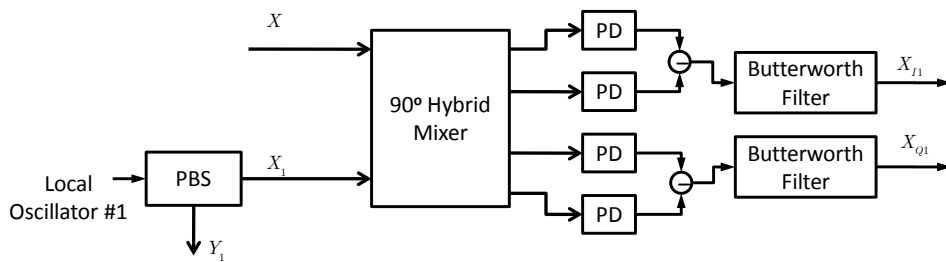
Figure 3.15: The block diagram of one homodyne receiver that is used in a dual carrier system.

Fig. 3.16 shows the ideal eye diagram of the in-phase of the X-component of one carrier for 100 Gb/s PM-QPSK at 50 GHz channel spacing with a large space (a) and with 20 GHz space (b) between the two carriers. In addition, Fig. 3.17 shows the ideal eye diagram of the in-phase of the X-component of one carrier for 400 Gb/s PM-

(a)

(b)
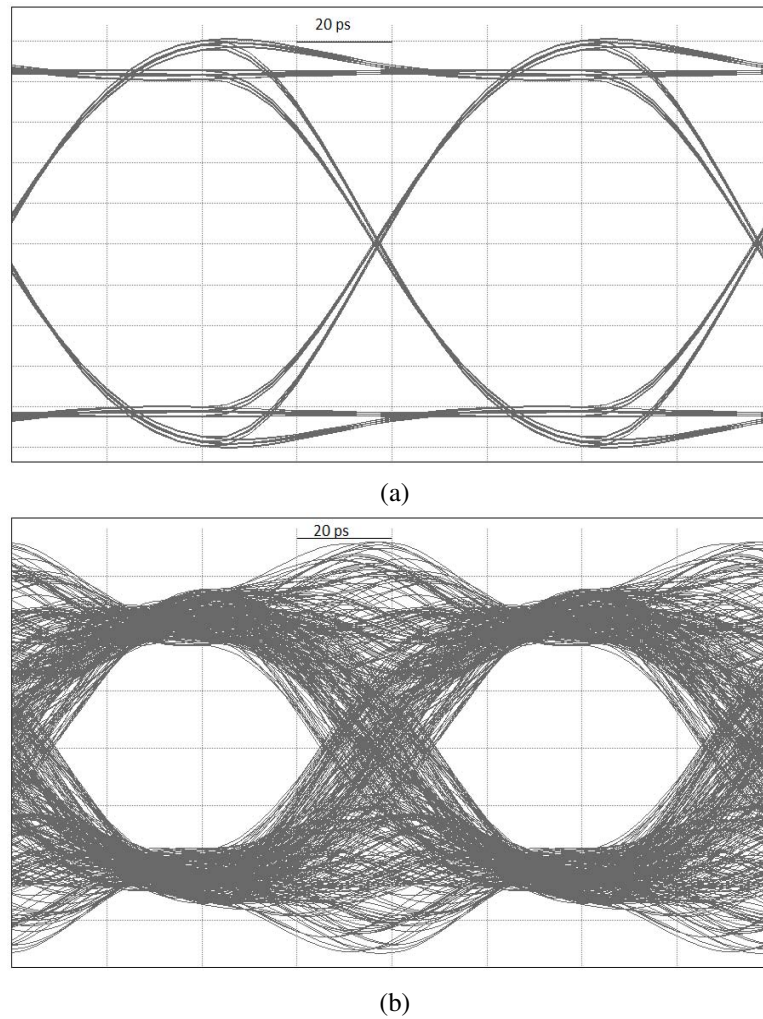
Figure 3.16: Eye diagram of ideal QPSK when the space between carriers assume to be (a) large space (b) 20 GHz space.

16QAM at 100 GHz channel spacing with a large space (a) and with 45 GHz space (b) between the two carriers.

We use VPI simulation tool [45] to model our simulation system that is shown in Fig. 3.18. Dual carrier transmitter and receiver are similar to the one explained before. The output of the dual carrier transmitter will pass through a cascaded filters with a central frequencies of f_0 before reaching the receiver. The two transmitters carrier frequencies (f_1 and f_2) are separated by 20 GHz (each laser is 10 GHz away from the filter's center frequency f_0) in terms of 100 Gb/s PM-QPSK with 50 GHz channel spacing. In addition, the two transmitters' carrier frequencies (f_1 and f_2) are separated by 45 GHz (each laser is 22.5 GHz away from the filter center's frequency f_0) in terms

46
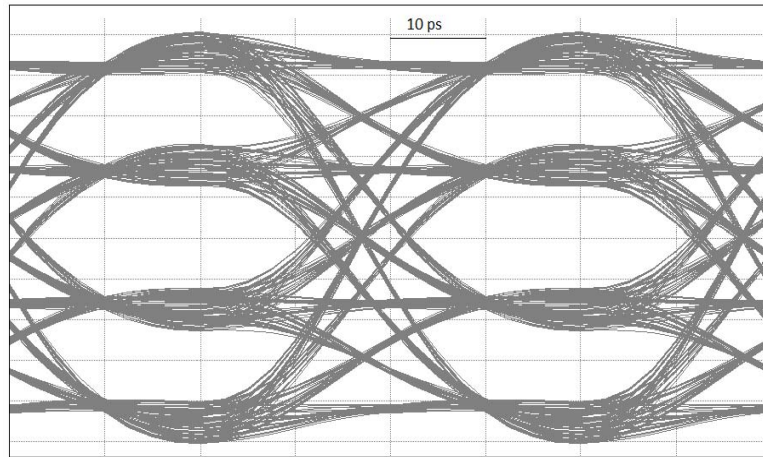
(a)
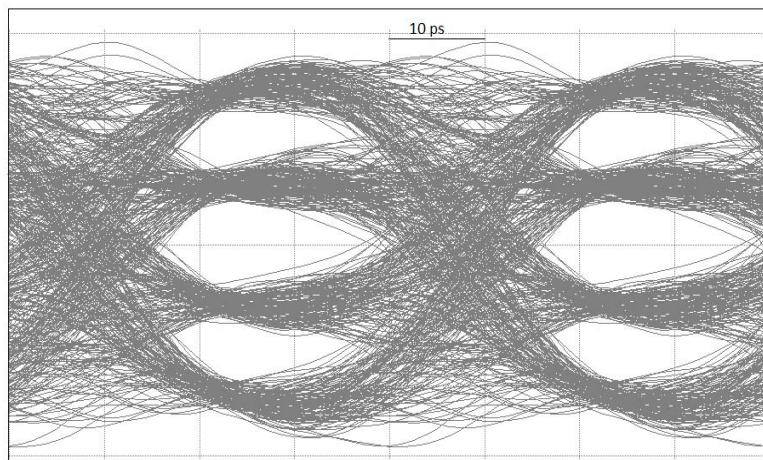
(b)

Figure 3.17: Eye diagram of ideal 16-QAM when the space between carriers assume to be (a) large space (b) 45 GHz space.

of 400 Gb/s PM-16QAM with 100 GHz channel spacing.
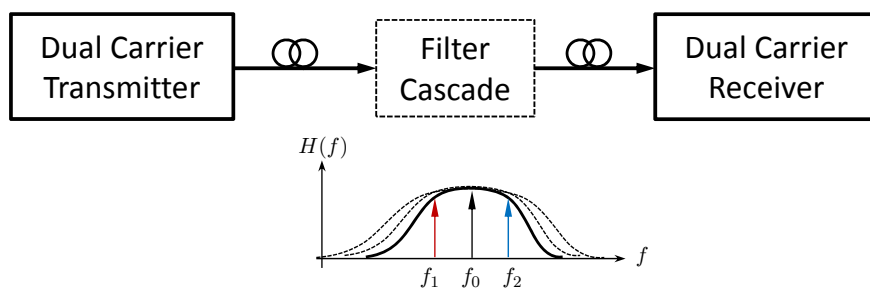
Figure 3.18: Simulation block diagram of a dual-carrier system.

3.4.2 Simulation Results

3.4.2.1 Dual-Carrier 100 Gb/s PM-QPSK System

In this section, we use the same FBG and TFF filters at 50 GHz channel spacing with 3-dB bandwidth of 43 GHz that are used in Section 3.3.2.1. Using simulation, the effect of cascading a number of FBG and TFF filters is studied on the in-phase of the *X*-component of one carrier. Fig. 3.19 shows the eye diagram when cascading two FBG and TFF filters. From the figure, we can notice that the eye opening corresponding to cascade two TFF filters is better than the one corresponding to two FBG filters cascade.
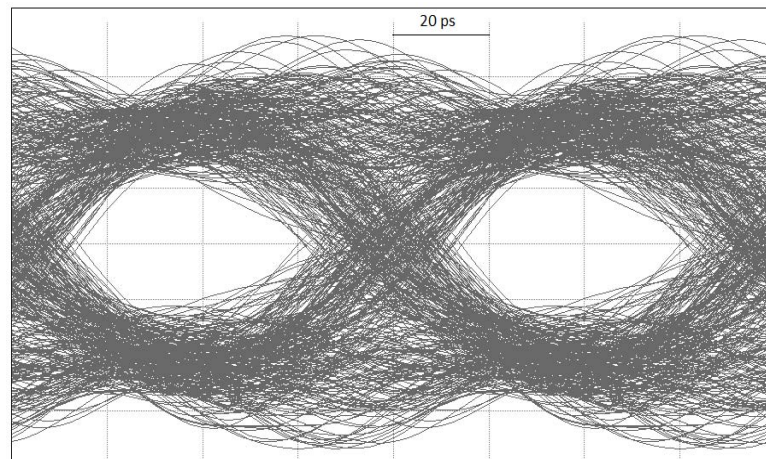
(a)
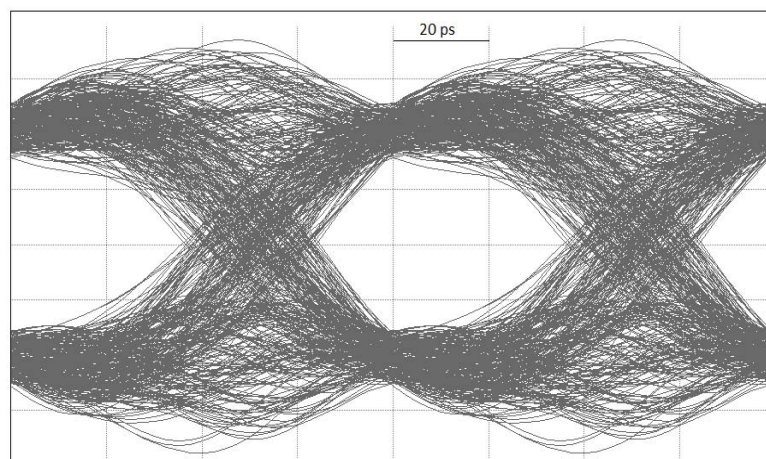
(b)

Figure 3.19: Eye diagrams when cascading two 43 GHz FBG (a) and TFF (b) at 50 GHz channel spacing for a dual carrier QPSK.

ECP has been calculated for a number of FBG and TFF filters. Fig. 3.20 shows the ECP versus the number of FBG and TFF with 3-dB bandwidth of 43 GHz at 50 GHz channel spacing. The results indicate that for 3-dB ECP, we can only cascade 2 TFF and 1 FBG filters, while at 6-dB ECP we can only cascade 4 TFF and 2 FBG filters. These results are shown in Table. 3.2.
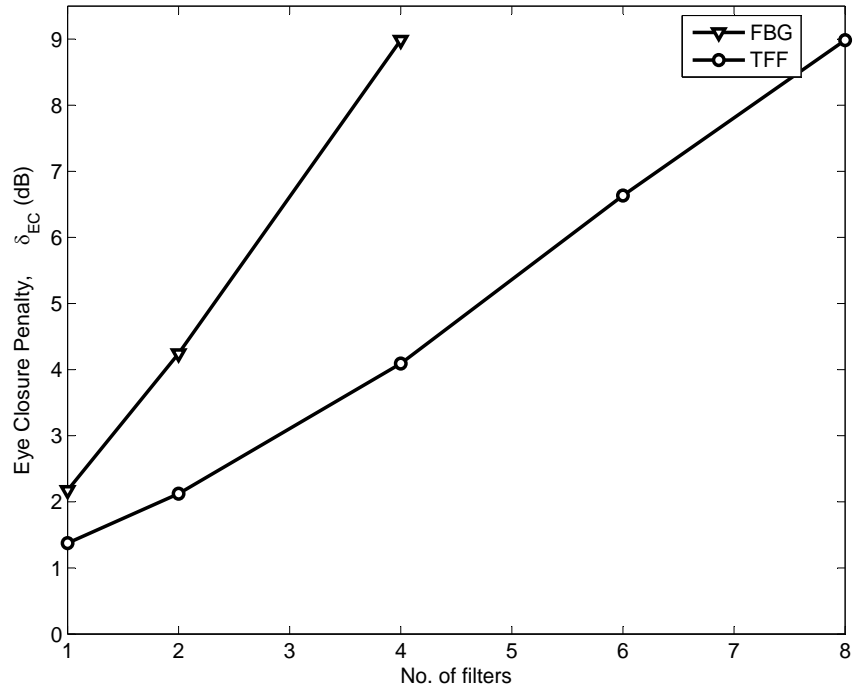
Figure 3.20: Eye closure penalty for 43 GHz FBG and TFF filters at 50 GHz channel spacing for dual carrier QPSK.

	No. of cascaded filters	
Filter Types	@ 3-dB ECP	@ 6-dB ECP
TFF 43 GHz	2	4
FBG 43 GHZ	1	2

Table 3.2: No. of filters at specific ECP for FBG and TFF in a dual carrier system with 50 GHz channel spacing.

3.4.2.2   Dual-Carrier 400 Gb/s PM-16QAM System

In this section, we use the same FBG and TFF filters at 100 and 150 GHz channel spacing with 3-dB bandwidth of 90 and 135 GHz that are used in Section 3.3.2.2. The effect of cascading a number of FBG and TFF filters is studied on the in-phase of the *X*-component of one carrier. Fig. 3.21 shows the eye diagram when cascading one FBG and TFF filters with 3-dB bandwidth of 90 at 100 GHz channel spacing. From the figure, we can notice that the eye opening corresponding to cascade one TFF filters is better than the one corresponding to one FBG filters cascade. Also, the resultant eye diagrams of cascading one FBG and TFF filters at 150 GHz channel spacing are shown in Fig. 3.22.

(a)

(b)
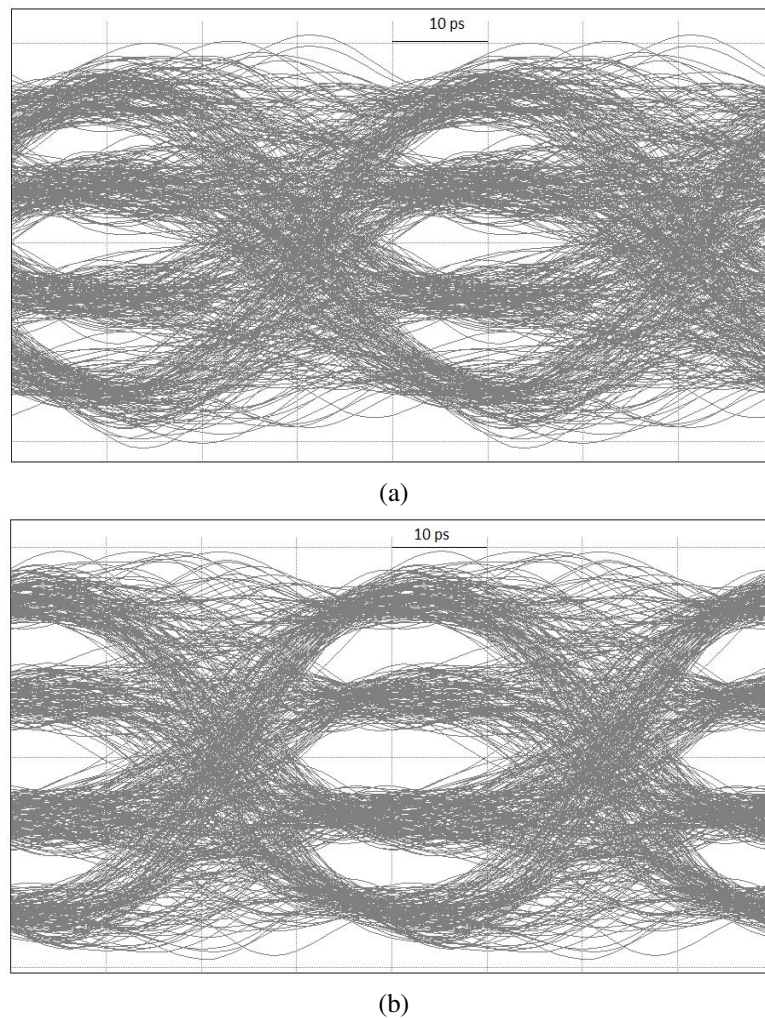
Figure 3.21: Eye diagrams when cascading one 90 GHz FBG (a) and TFF (b) at 100 GHz channel spacing for a dual carrier 16-QAM.

50

(a)

(b)
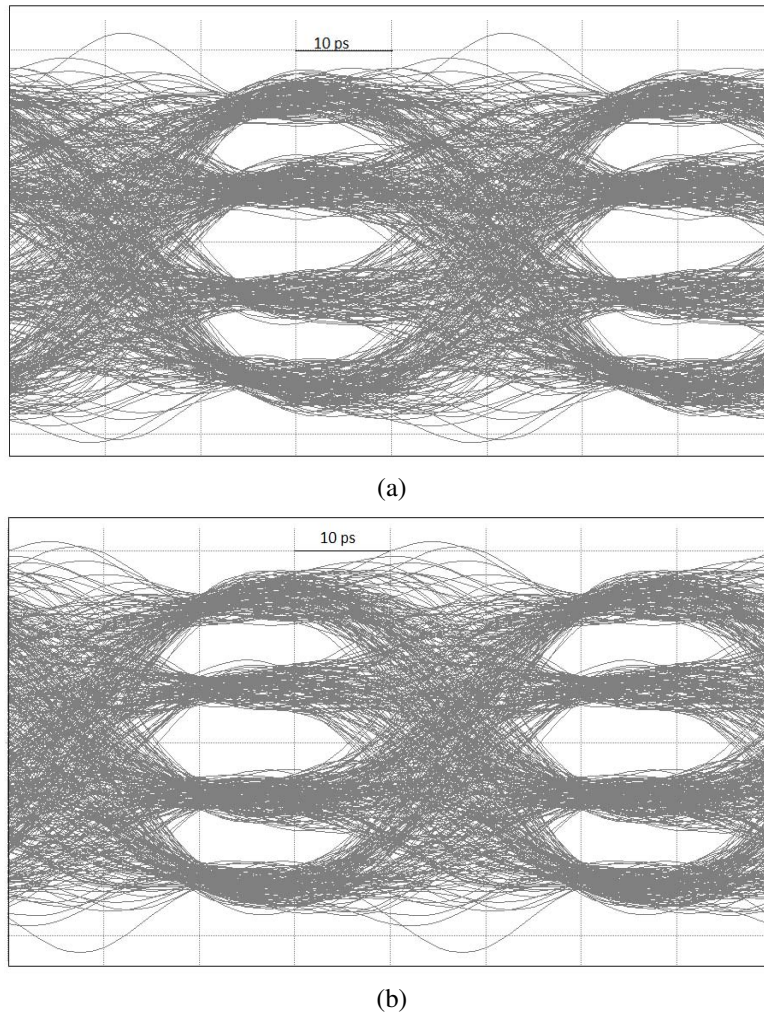
Figure 3.22: Eye diagrams when cascading one 135 GHz FBG (a) and TFF (b) at 150 GHz channel spacing for a dual carrier 16-QAM.

ECP is shown in Fig. 3.23 as a function of the number of FBG and TFF at 100 and 150 GHz channel spacing. Simulation results indicate that for 6-dB ECP, we can only cascade a single TFF filter at 100 GHz channel spacing with 3-dB bandwidth of 90 GHz.

Moreover, FBG and TFF filters are used with 3-dB bandwidth of 135 GHz at channel spacing of 150 GHz. The results indicate that at 6-dB ECP, we can only cascade 4 TFF and a single FBG filters. Table. 3.3 and Table. 3.4 provide a summary of the results.

When comparing the results of filter cascading for a single-carrier and a dual-carrier 100 Gb/s PM-QPSK and 400 Gb/s PM-16QAM, the results indicate that dual-carrier

51
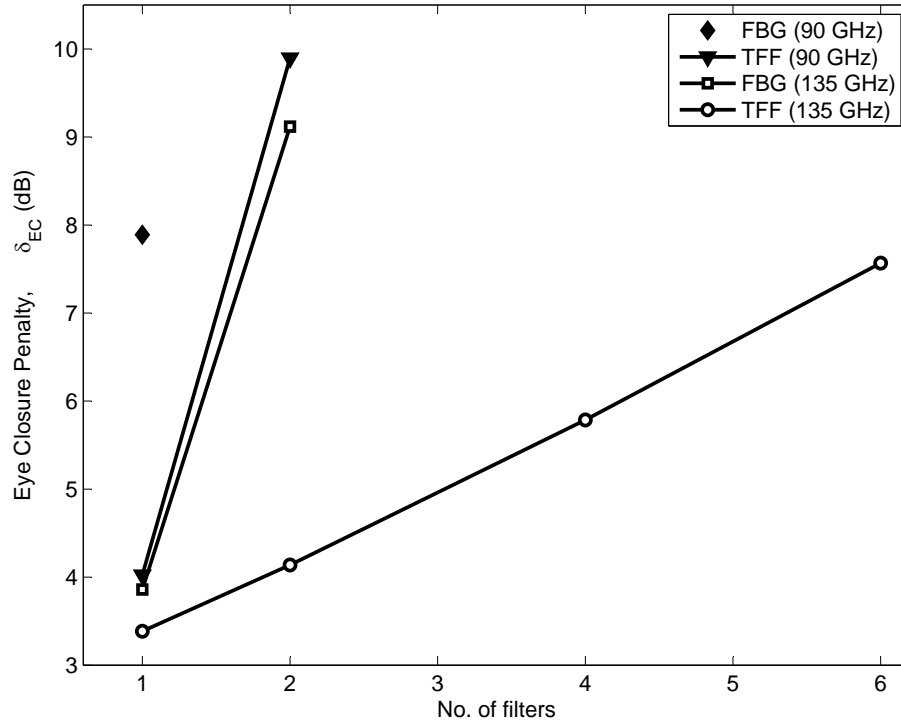
Figure 3.23: Eye closure penalty for 90 GHz and 135 GHz FBG and TFF filters for a dual carrier 16-QAM.

No. of filters	1	2
TFF 90 GHz	4.024	9.897
FBG 90 GHz	7.889	-

Table 3.3: ECP (in dB) for a number of FBG and TFF in a dual carrier system with 100 GHz channel spacing.

No. of filters	1	2	4	6
TFF 135 GHz	3.386	4.138	5.786	7.568
FBG 135 GHz	3.859	9.118	-	-

Table 3.4: ECP (in dB) for a number of FBG and TFF in a dual carrier system with 150 GHz channel spacing.

transmission systems are worse than single-carrier transmission system in terms of the number of filters that the WDM signal can pass through.

The reason for this is that in dual-carrier transmission systems, both carriers are shifted from the filter's center frequency and there is a crosstalk effect between the two carriers.

Chapter 4

Chromatic Dispersion Equalization for 100 Gb/s PM-QPSK and 400 Gb/s PM-16QAM Using FD-FIR Filter

4.1   Introduction

The performance of a high speed transmission systems is severely affected by CD. DCFs are commonly used to compensate for this kind of distortion but they are considered an expensive and bulky solution. Digital coherent receivers allow equalization for linear transmission impairments in the electrical domain, which means that it is possible to compensate for CD with zero penalty in digital coherent receivers by using electronic dispersion compensation (EDC) techniques. Several digital filters were used to compensate for CD in time and frequency domains. In this thesis, we are interested in time domain equalization using a fiber-dispersion finite impulse response (FD-FIR) filter.

4.2   Related Works

Many research groups show interest in EDC techniques that are used in coherent receivers such as analog equalizers, digital filters and maximum likelihood sequence estimation (MLSE) equalizers.

A digital coherent receiver is similar to a conventional coherent receiver except that

it employs a DSP in order to compensate for dispersion and recover the phase of the signal. This is achieved by converting the signal from analog to digital, where it will be applied to one of equalization techniques.

The first CD equalizer was proposed by [32] using the MLSE method for an OOK system. The MLSE equalizer is implemented by using the Viterbi algorithm, where one is looking for the most likely bit sequence formed by a series of distorted signals. The MLSE is optimum for any kind of optically distorted signal detected by a PD, given that inter-symbol interference is not exceeded specific threshold.

The first CD equalizer based on FIR filter was proposed by [33]. FIR filter with various number of taps (19 and 39 taps for 100 and 200 km; respectively) was implemented in a DSP circuit after homodyne detection and has been used to compensate for group-velocity dispersion of an unrepeated optical transmission of 20 Gb/s QPSK over 200 km long SMF.

A distance of 6400km has been experimentally achieved in [34],[35] for a 42.8 Gb/s QPSK system using a digital coherent receiver with FIR filter of 512 taps. This was considered the first time of transmitting 40 Gb/s over such a distance on standard fiber, without the use of optical dispersion compensation and it exceeded the previously reported distance for 10 Gb/s systems.

A time domain FD-FIR was used by [36] to compensate for the CD of 42.8 Gb/s transmission over 1000 and 4000 km fiber without using DCFs. It provided a design for a digital FD-FIR filter from the digitalization of the time domain impulse response of the inverse of the fiber's transfer function.

The time window of the FD-FIR filter can be truncated by using the Nyquist frequency, which is determined to avoid the aliasing phenomenon in the digital systems. The analytical truncated impulse response method for the design a digital FIR filter allows compensation of arbitrary amounts of CD.

An adaptive FIR digital filter based on normalized least mean square (NLMS) algorithm was proposed by [39],[40]. The adaptive FIR filter was developed to compensate for CD in a 112 Gb/s PM-QPSK transmission system. This filter makes an update for

the filter taps after equalizing the incoming sample, so it requires slow iteration for guaranteed convergence.

A few researches have been performed on equalization using IIR since it is difficult to analyze and add complexity at the receiver side. Digital IIR filtering was proposed [41] as a means for compensating CD in homodyne-detected optical transmission systems with subsequent digital signal processing. Compared to FIR filtering, IIR filtering achieves dispersion compensation using a significantly smaller number of taps. Dispersion compensation of 80 and 160 km in a 10 Gb/s binary phase shift keying (BPSK) was experimentally compared for the two filtering schemes. The results indicated that IIR filtering can achieve performance similar to the FIR filtering scheme but with lower number of taps.

4.3   Dispersion Compensation Filter Design

Since in our work we are only considering the CD and assume there is no PMD or fiber non-linear effects, the CD is a linear operation on the electrical field, and its effect can be undone by linear filtering. So we propose to compensate for specific amount of CD using FD-FIR filter.

The transfer function of the fiber with CD given by [42]

$$H_{disp}(f) = \exp\left(j\alpha f^2\right), \alpha = \frac{D\lambda^2 \pi z}{c} \tag{4.1}$$

Where D is the fiber dispersion coefficient and given by:

$$D(\lambda) = \frac{1}{z}\frac{\partial \tau}{\partial \lambda} \tag{4.2}$$

Where τ is the fiber group delay, and for $\lambda = 1550$ nm D = 17 $ps/(nm.km)$. λ is the central wavelength of the transmitted signal and z is the transmitted distance.

By taking the Inverse Fourier Transform for $\exp\left(-j\alpha f^2\right)$, the impulse response

function of the compensating filter is expressed as:

$$h_{eq}(t) = \sqrt{\frac{-jc}{D\lambda^2 z}} \exp\left(j\phi(t)\right) \text{ ,where } \phi(t) = \frac{\pi c}{D\lambda^2 z} t^2 \tag{4.3}$$

According to [36], the impulse response of the dispersion compensating filter is infinite in duration, non-causal and aliasing will occur because it passes all frequencies for a finite sampling frequency.

The solution to all of these problems [36] is to truncate the impulse response to a finite duration, where the time window of the FD-FIR filter should be truncated by using the Nyquist frequency that is given by $\omega_n = \pi/T$, where T is the sampling period. When the Nyquist frequency is exceeded, aliasing occurs and impulse response may be considered as a rotating vector where its angular frequency is given by:

$$\omega = \frac{\partial \phi(t)}{\partial t} \tag{4.4}$$

$$= \frac{2\pi c}{D\lambda^2 z} t \tag{4.5}$$

after truncating the impulse response using Nyquist frequency, the impulse response becomes of finite duration as:

$$-\frac{|D|\lambda^2 z}{2cT} \le t \le \frac{|D|\lambda^2 z}{2cT} \tag{4.6}$$

Now since the impulse response is of finite duration, we can implement this digitally using FD-FIR filter as follows:

$$h_{eq}[n] = \sum_{k=-N/2}^{N/2} b_k \delta(n-k) \tag{4.7}$$

Where b_k is the tap weights and given by:

$$b_k = \sqrt{\frac{-jcT^2}{D\lambda^2 z}} \exp\left(j\frac{\pi cT^2}{D\lambda^2 z} k^2\right) \ ; -\left\lfloor \frac{N}{2} \right\rfloor \le k \le \left\lfloor \frac{N}{2} \right\rfloor \tag{4.8}$$

Where N is the number of taps for a CD compensating filter, and is expressed as follows:

$$N = 2 \times \left\lfloor \frac{|D|\lambda^2 z}{2cT^2} \right\rfloor + 1 \qquad (4.9)$$

Where $\lfloor x \rfloor$ is the nearest integer less than x.

4.4 System Model

The CD equalization system model used in our simulation consists of a transmitter, fiber channel and coherent receiver that employing a CD compensating filter.

The transmitter that is used in our simulation is the same to the one that has been described and shown in Fig. 3.3, Section. 3.3.

The focus of this section is to simulate the CD effects on the transmitted signal without any consideration of the PMD and non-linear effects of a transmission fiber. So, we will only analyze the X-component of the signal passing through the fiber.
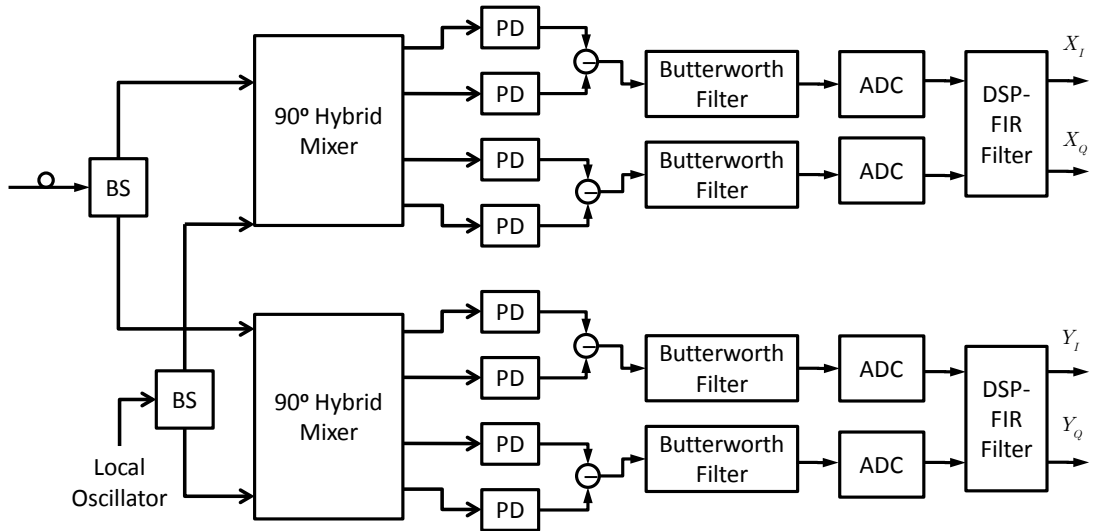
Figure 4.1: Block diagram of the optical homodyne receiver employing FIR filter.

We consider a homodyne receiver as shown in Fig. 4.1 with an ideal LO synchronized to the X-component. The LO and the received signal are applied to 90° hybrid mixer, where the in-phase and the quadrature-phase signals of the X-component are demodulated using four PDs.

The current from PD is filtered by a third order Butterworth electric filter that has a 3-dB bandwidth of 65% of the symbol rate to reduce the noise and prevent aliasing. Then the outputs of electric filters are digitalized using analog-to-digital converters (ADCs) at twice or four times the symbol rate, where today's ADCs operate at 100 GSamples/s (Tektronix MSO70000) [46]. After this, the sampled signals are processed by FIR filter to equalize for CD. Finally, BER based on Monte-Carlo (MC) technique is estimated from the data sequence.

4.5 Simulation Results

This section shows the results for CD equalization for both 100 Gb/s PM-QPSK and 400 Gb/s PM-16QAM systems. For each system, we used 2 and 4 samples/symbol to compensate for CD and compared the results for each system.

4.5.1 CD Equalization for 100 Gb/s PM-QPSK

4.5.1.1 Equalization using 2 samples/symbol

We have used the equations in Section. 4.3 to compute the number of taps required to compensate for CD for multiple distances using 2 samples/symbol. Table. 4.1 shows the maximum number of taps (N_{max}) that the FD-FIR filter required to compensate for specific amount of dispersion. From the table, we can notice that number of taps is increased linearly as it is linearly dependent on the propagation distance.

Distance (km)	N_{max}
500	171
1000	341
2000	683
3000	1025
4000	1367

Table 4.1: Maximum number of taps for FD-FIR compensating filter for 100 Gb/s PM-QPSK using 2 samples/symbol.

Fig. 4.2 shows the ideal eye diagram of QPSK and the equalized eye diagrams after certain distances. To have a clear validation of the CD compensating filter, we have generated BER versus OSNR curves. The OSNR at the receiver is relative to the equivalent amplifier cascade noise measured in a bandwidth of 0.1 nm. Fig. 4.3 shows a typical system that goes from transmitter to receiver, where each 100 km fiber is followed by an amplifier. The amplifier's noise power is defined as the noise power measured in 0.1nm of bandwidth at the receiver input.

We have generated BER versus OSNR curve for back-to-back (0 km) and after CD compensation for 1000 km and 4000 km fiber length, where the BER was measured over a total bits of 262144 bits for different OSNR values.

Fig. 4.4 shows BER versus OSNR curve for back-to-back and after the CD compensating for 1000 km and 4000 km fiber length using maximum number of taps. From Fig. 4.4, we can see that there is no penalty between back-to-back curve and the curves that are associated with the compensation of CD when using the maximum number of taps given by Eq. 4.8 and Eq. 4.9.

Furthermore, we tried to reduce the number of taps that is used in designing the FIR filter to 75% and 50% of the maximum number of taps and determine if there is an effect on the performance of the equalized signal. The results in Fig. 4.5 indicate that there is a minor penalty when using 75% of the maximum number of taps while there a significant penalty when using only 50% of the maximum number of taps. Table. 4.2 shows the OSNR penalty (at BER of 10^{-3} relative to back-to-back) when using 75% and 50% of the maximum number of taps, given that the back-to-back OSNR level required for a BER of 10^{-3} (this BER limit value allows a full error recovery using forward error correction techniques to have BER better than 10^{-15} [44]) is 14.4 dB.

The results indicate that using 75% of the maximum number of taps has minimal impact on the performance, which results in an OSNR penalty of 0.24 and 0.22 dB for 1000 and 4000 km, respectively. While making a significant reduction in the number of taps (using 50% of the maximum number of taps) has notable effect on performance, this results in an OSNR penalty of 1.42 and 1.33 dB for 1000 and 4000 km, respectively.

(a)

(b)

(c)

(d)

(e)

(f)
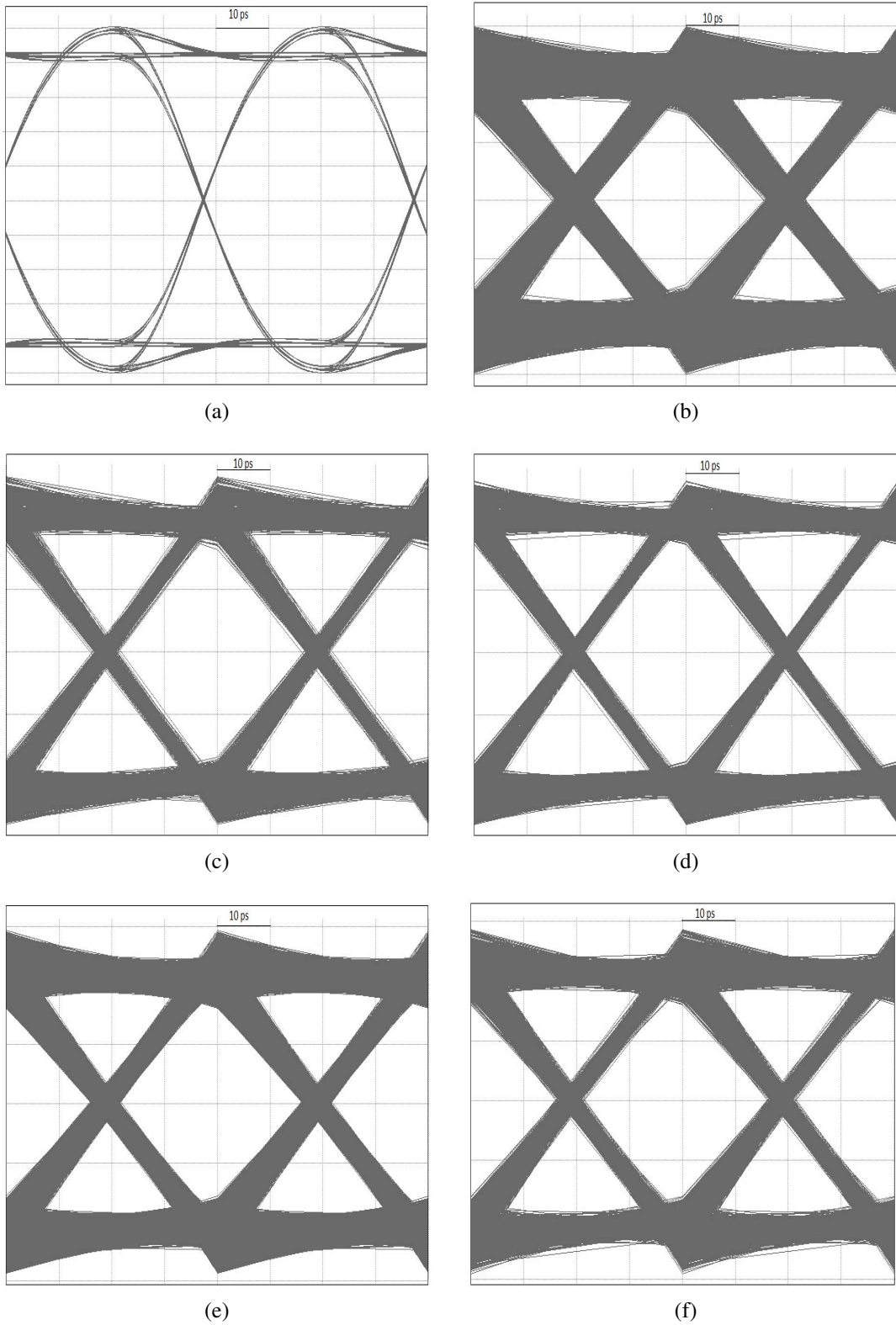
Figure 4.2: Eye diagram of ideal QPSK (a) and the eye diagrams after CD equalization for distances: 500 km (b), 1000 km (c), 2000 km (d), 3000 km (e), 4000 km (f) using 2 samples/symbol.

Figure 4.3: Schematic diagram for a cascade of fiber and amplifier.
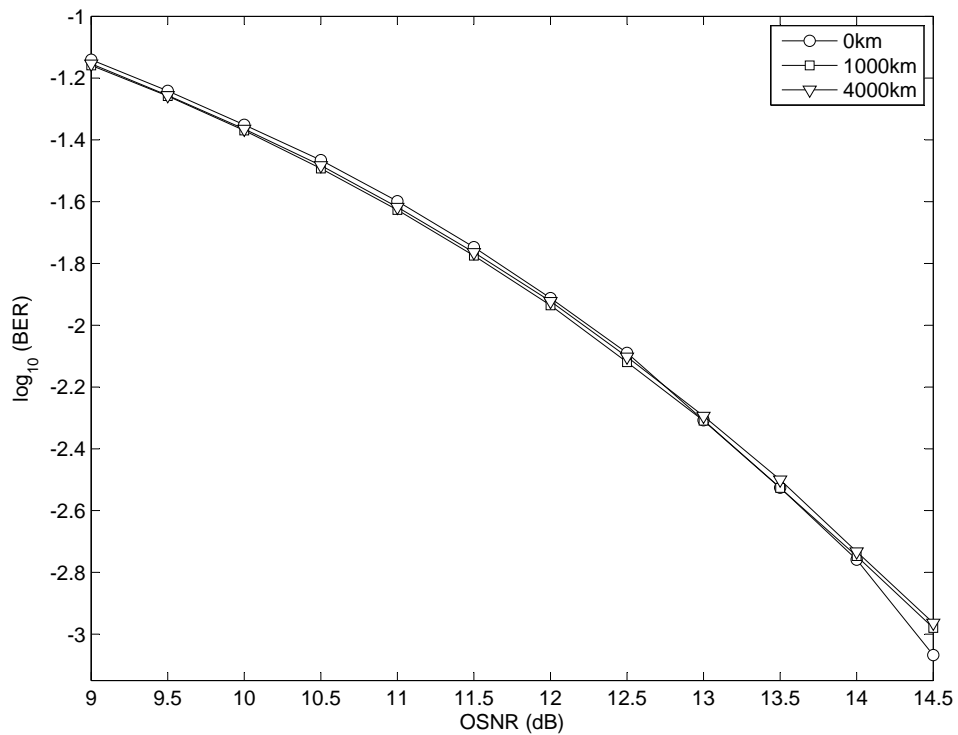
Figure 4.4: BER versus OSNR for QPSK using 2 samples/symbol with maximum number of taps.

Distance (km)	OSNR Penalty (dB) using 75%	OSNR Penalty (dB) using 50%
1000	0.24	1.42
4000	0.22	1.33

Table 4.2: OSNR penalty of equalized QPSK signal using 2 samples/symbol with 75% and 50 % of the maximum number of taps at BER of 10^{-3}.
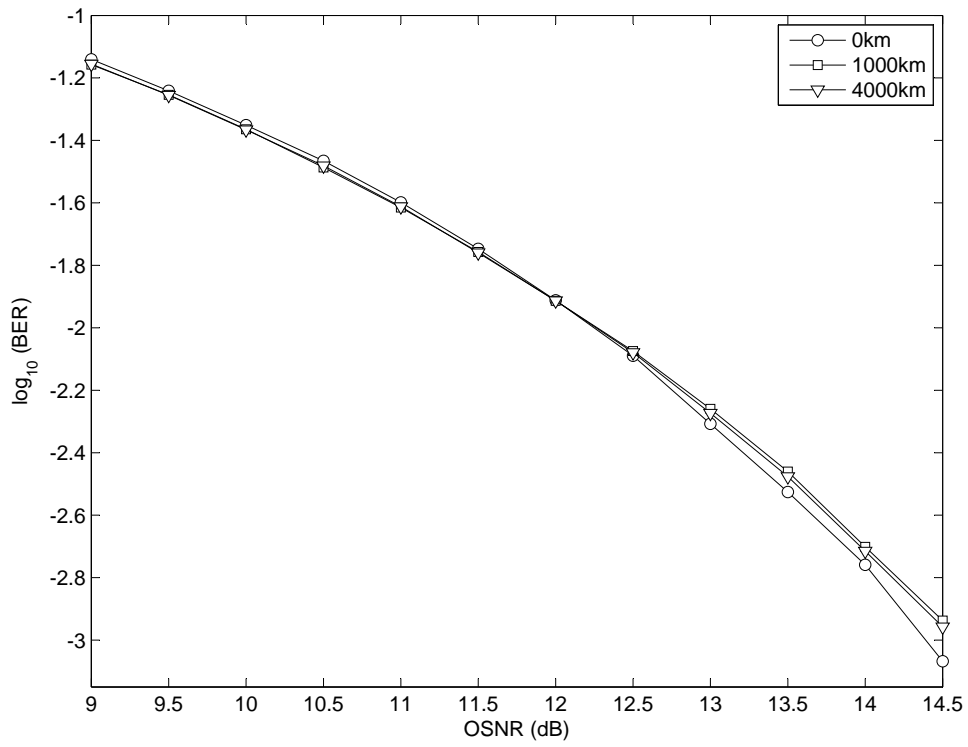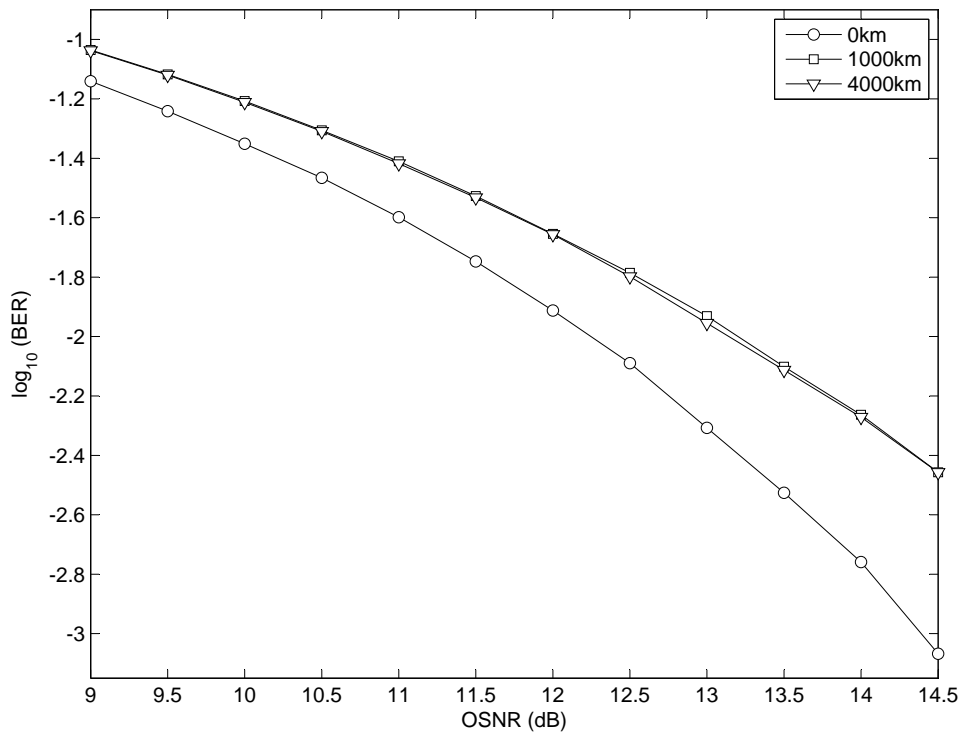
Figure 4.5: BER versus OSNR for QPSK using 2 samples/symbol with (a) 75% (b) 50% of the maximum number of taps.

4.5.1.2 Equalization using 4 samples/symbol

We computed the number of taps required to compensate for CD for multiple distances using 4 samples/symbol using Eq. 4.8 and Eq. 4.9. Table. 4.3 below shows the maximum number of taps that the FD-FIR filter required to compensate for a specific amount of CD. The results indicate that the number of taps is increased linearly as it is linearly dependent on the propagation distance.

Distance (km)	N_{max}
500	683
1000	1367
2000	2733
3000	4101
4000	5467

Table 4.3: Maximum number of taps for FD-FIR compensating filter for 100 Gb/s PM-QPSK using 4 samples/symbol.

Fig. 4.6 shows the equalized eye diagrams after certain distances. From the figure, we can notice that there is a difference between the equalized eye diagrams when using 2 and 4 samples/symbol. To have a clear validation of the CD compensating filter and a clear comparison, we have also generated an BER versus OSNR curves.

We have generated BER versus OSNR curve for back-to-back (0 km) and after CD compensation for 1000 km and 4000 km. From Fig. 4.7, we can see that there is no penalty between back-to-back curve and the curves that are associated with the compensation of CD when using the maximum number of taps given by Eq. 4.8 and Eq. 4.9. Also, the results seem to be similar when using 2 samples/symbol with maximum number of taps.

Furthermore, we tried to reduce the number of taps that is used in designing FD-FIR filter to 75% and 50% of the maximum number of taps and determine if there is an effect on the performance of the equalized signal. The results are shown in Fig. 4.8 indicates that there is no notable penalty when using 75% and 50% of the maximum number of taps; in fact, it's even performing better compared to using the maximum number of
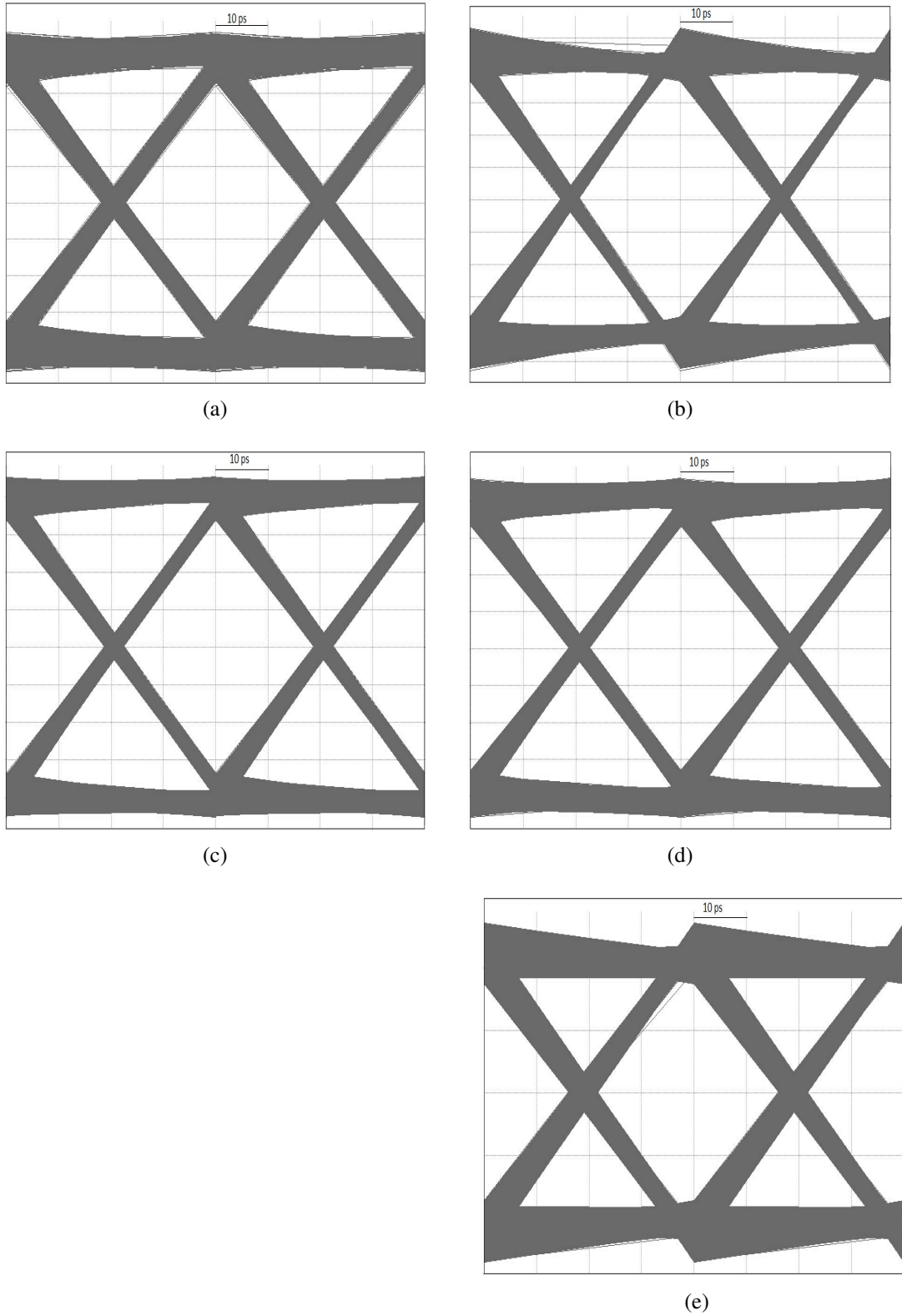
Figure 4.6: Eye diagrams after CD equalization for distances: 500 km (a), 1000 km (b), 2000 km (c), 3000 km (d), 4000 km (e) using 4 samples/symbol.

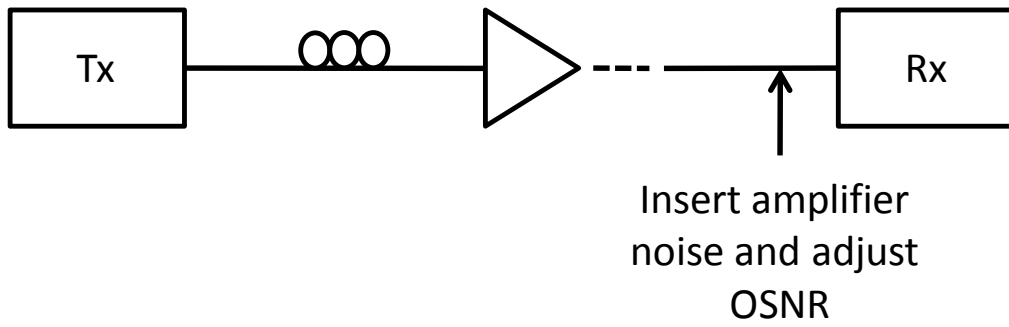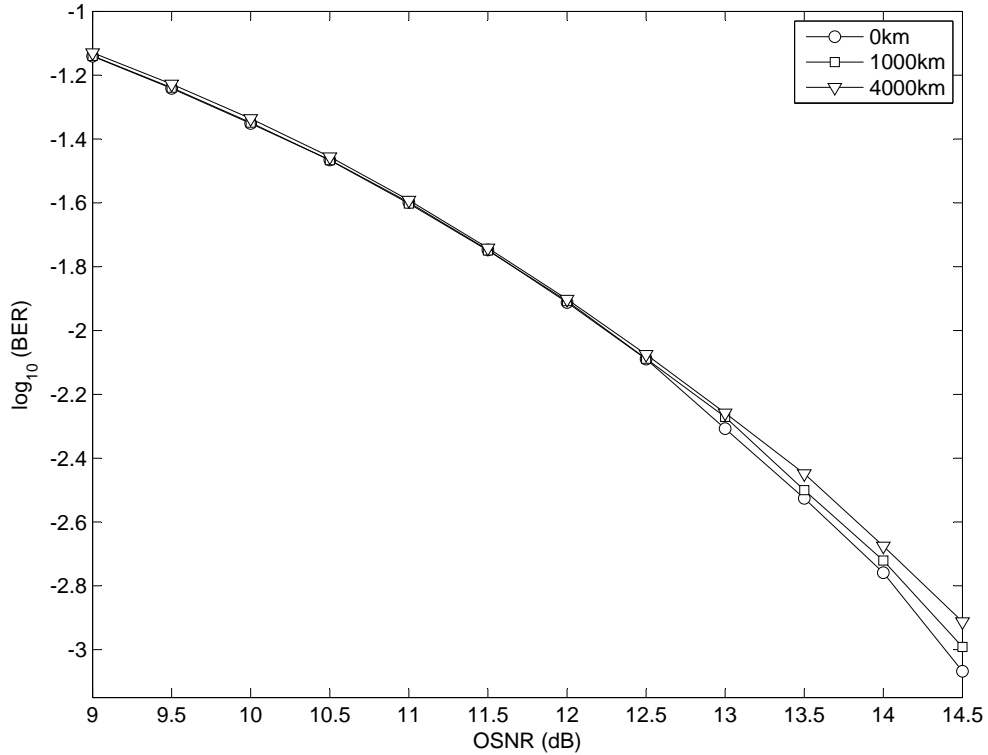Figure 4.7: BER versus OSNR for QPSK using 4 samples/symbol with maximum number of taps.

taps. When comparing the results of CD equalization using 2 samples/symbol and 4 samples/symbol, we can notice that there is no difference in performance when using the maximum number of taps. In addition, when we reduce the number of taps in terms of 4 samples/symbol to 50% of the maximum number (which is approximately twice the maximum number of taps using 2 samples), there is no notable difference in terms of OSNR penalty . This indicates that for CD equalization in 100 Gb/s PM-QPSK, using 2 samples/symbol is the best approach to compensate for CD.
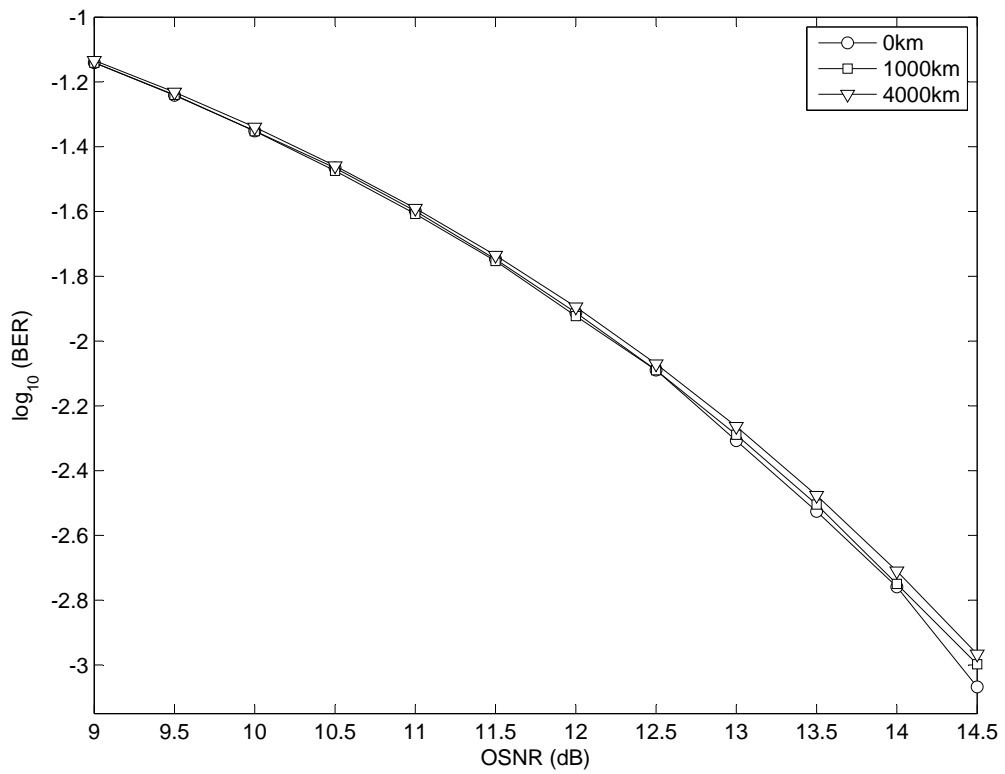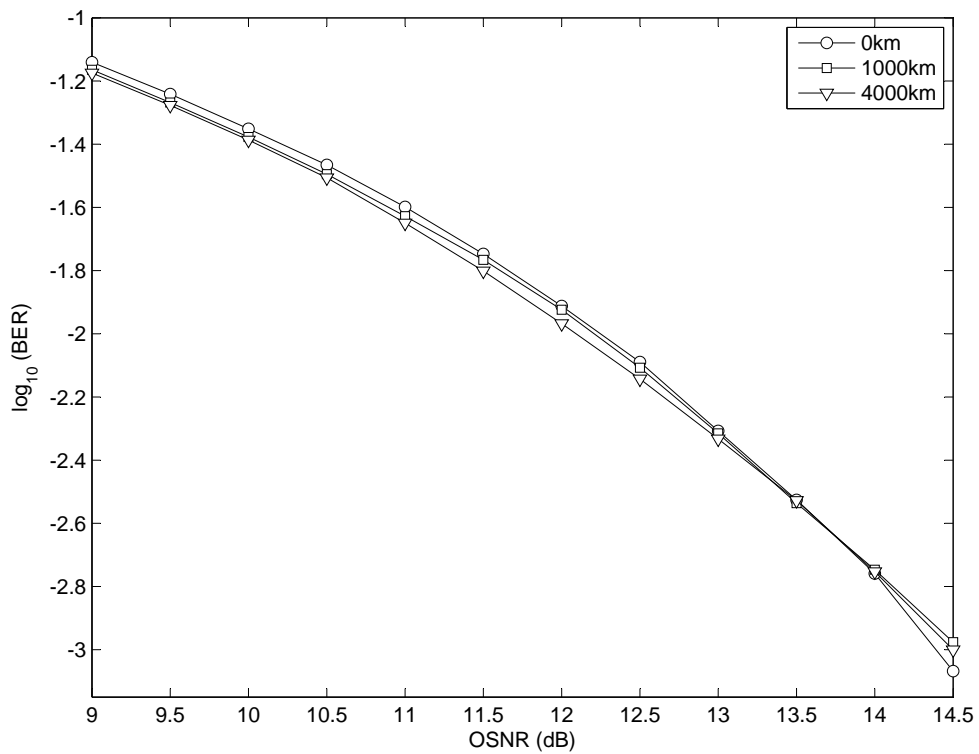
Figure 4.8: BER versus OSNR for QPSK using 4 samples/symbol with (a) 75% (b) 50% of the maximum number of taps.

4.5.2 CD Equalization for 400 Gb/s PM-16QAM

4.5.2.1 Equalization using 2 samples/symbol

We have used the equations in Section. 4.3 to compute the number of taps required to compensate for CD for multiple distances using 2 samples/symbol. Table. 4.4 shows the maximum number of taps that the FD-FIR filter required to compensate for specific amount of dispersion. From the table, we can notice that number of taps is increased linearly as it is linearly dependent on the propagation distance.

Distance (km)	N_{max}
200	273
500	683
1000	1367

Table 4.4: Maximum number of taps for FD-FIR compensating filter for 400 Gb/s PM-16QAM using 2 samples/symbol.

Fig. 4.9 shows the ideal eye diagram of 16-QAM and the equalized eye diagrams after a certain distances. To have a clear validation of CD compensating filter, we have generated BER versus OSNR curves.

We have generated BER versus OSNR curve for back-to-back (0 km) and after CD compensation for 500 km and 1000 km. From Fig. 4.10, we can see that there is a notable penalty between back-to-back curve and the other curves especially the curve that is associated with 1000 km after compensating for CD using the maximum number of taps given by Eq. 4.8, Eq. 4.9.

Furthermore, when reducing the number of taps that is used in designing FD-FIR filter to 75% and 50% of the maximum number of taps, the OSNR penalty has been increased to higher level. The results are shown in Fig. 4.11 when using 75% and 50% of the maximum number of taps. Table. 4.5 shows the OSNR penalty when using the maximum number of taps, also for 75% and 50% of the maximum number of taps (at BER of 10^{-3} relative to back-to-back), given that the back-to-back OSNR level required
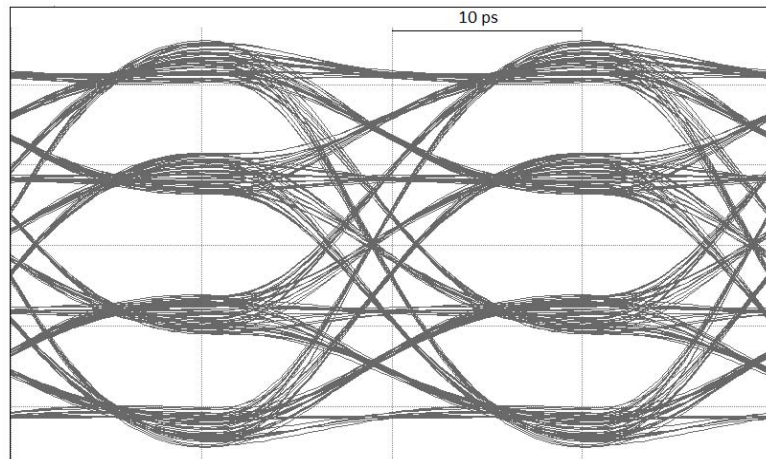
(a)
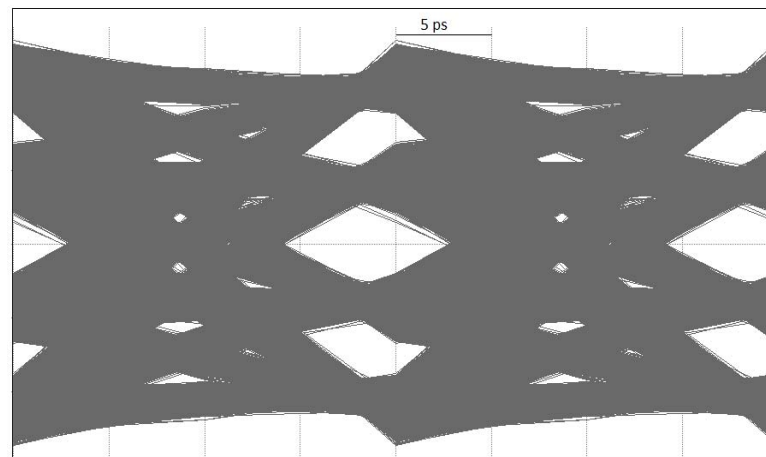
(b)
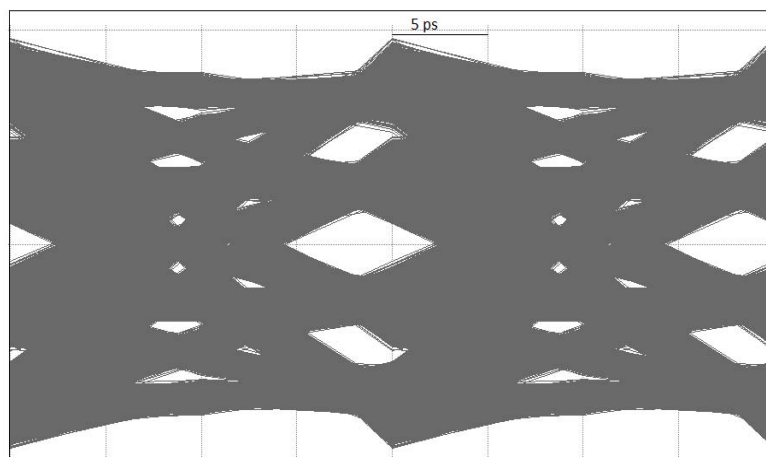
(c)

Figure 4.9: Eye diagram of ideal 16-QAM (a) and the eye diagrams after CD equalization for distances: 500 km (b), 1000 km (c) using 2 samples/symbol.
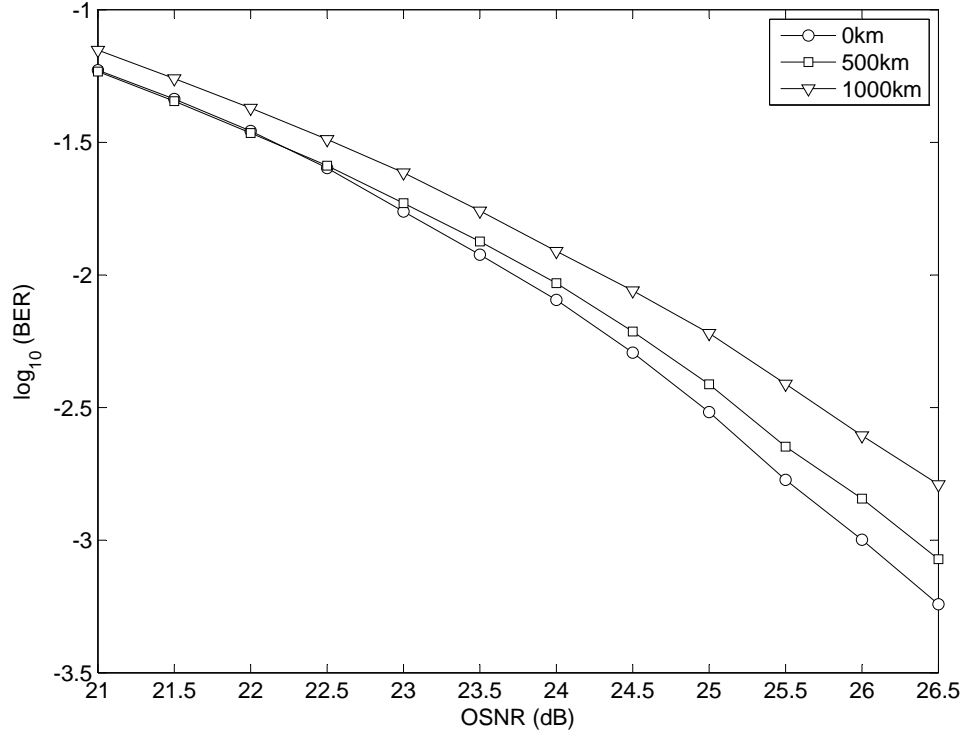
Figure 4.10: BER versus OSNR for 16-QAM using 2 samples/symbol with maximum number of taps.

for a BER of 10^{-3} (this BER limit value allows a full error recovery using forward error correction techniques to have BER better than 10^{-15} [44]) is 26 dB.

The results indicate that using the maximum number of taps results in an OSNR penalty of 0.4 and 0.95 dB for 500 and 1000 km, respectively. However, reducing the number of taps to 75% and 50% of the maximum number has a severe impact on performance. This means that using the maximum number of taps with 2 samples/symbol gives acceptable results when compensating for CD for 400 Gb/s PM-16QAM system.

Distance (km)	OSNR penalty (dB) using N_{max}	OSNR penalty (dB) using 75% of N_{max}	OSNR penalty (dB) using 50% of N_{max}
500	0.4	1.9	> 1.9
1000	0.95	2.5	> 2.5

Table 4.5: OSNR penalty of equalized 16-QAM signal using 2 samples/symbol with maximum number of taps, 75% and 50 % of the maximum number of taps at BER of 10^{-3}.
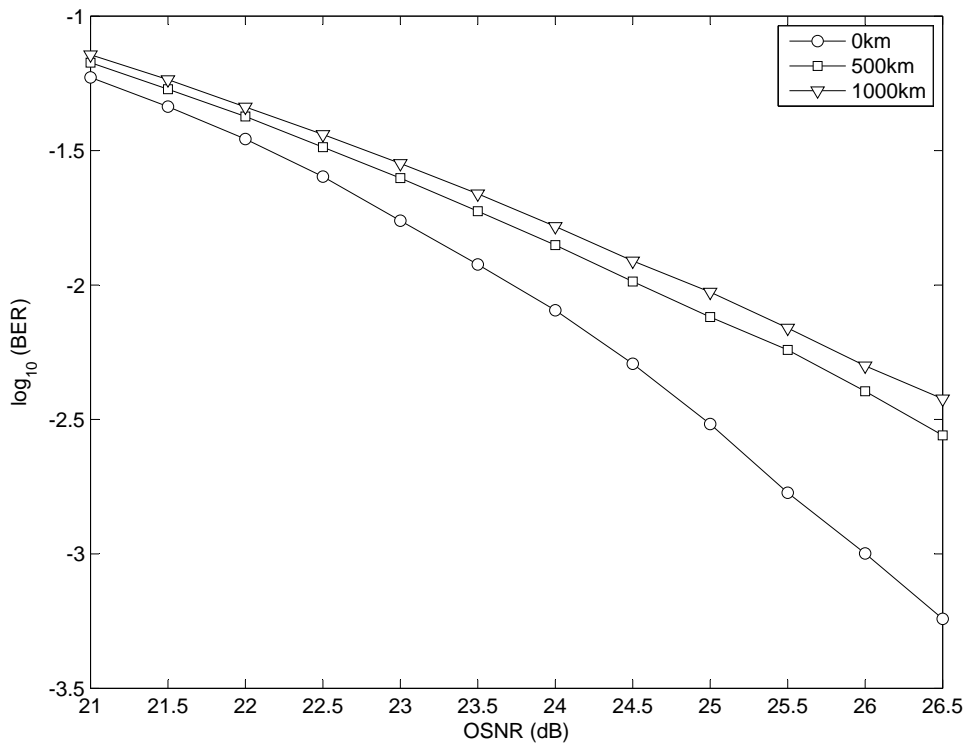
(a)
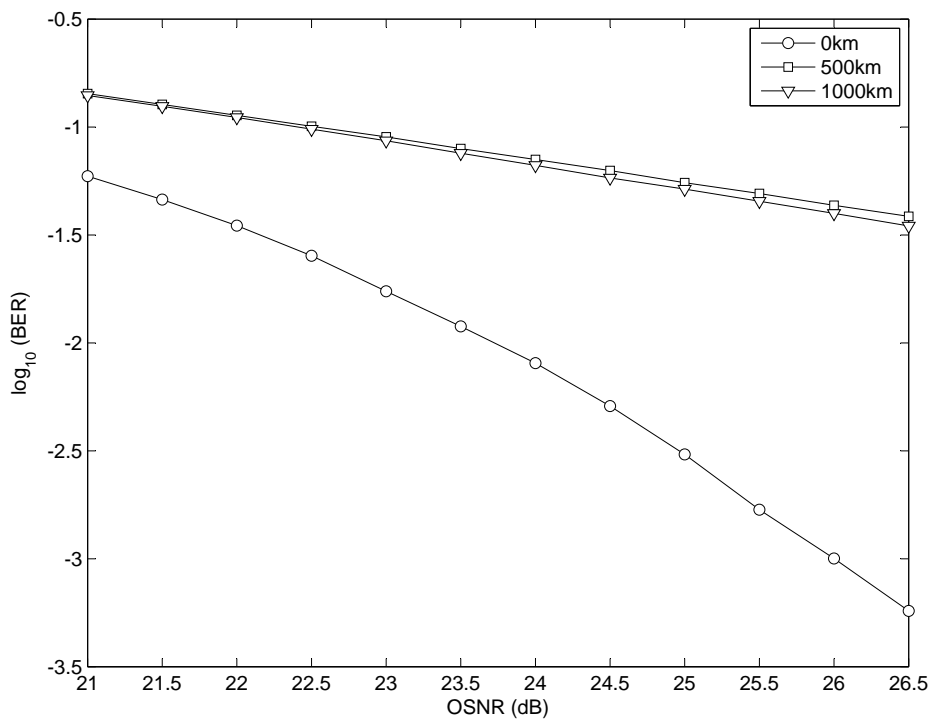
(b)

Figure 4.11: BER versus OSNR for 16-QAM using 2 samples/symbol with (a) 75% (b) 50% of the maximum number of taps .

4.5.2.2   Equalization using 4 samples/symbol

We compute the number of taps required to compensate for CD for multiple distances using 4 samples/symbol using Eq. 4.8 and Eq. 4.9. Table. 4.6 below shows the maximum number of taps that the FD-FIR filter required to compensate for a specific amount of CD. The results indicate that the number of taps is increased linearly as it is linearly dependent on the propagation distance.

Distance (km)	N_{max}
200	1093
500	2733
1000	5467

Table 4.6: Maximum number of taps for FD-FIR compensating filter for 400 Gb/s PM-16QAM using 4 samples/symbol.

Fig. 4.12 shows the equalized eye diagrams after certain distances. From the figure, we can notice that there is a clear difference between the equalized eye diagrams when using 2 and 4 samples/symbol. To have a clear validation of CD compensating filter and a clear comparison, we have also generated BER versus OSNR curves.

We have generated BER versus OSNR curve for back-to-back (0 km) and after CD compensation for 500 km and 1000 km. From Fig. 4.13, we can see that there is no notable penalty between the back-to-back curve and the 500 km curve while there is a small difference between the back-to-back curve and the curve that is associated with the compensation of CD of 1000 km fiber when using the maximum number of taps .

Furthermore, we tried to reduce the number of taps that is used in designing the FD-FIR filter to 75% and 50% of the maximum number of taps and determine if there is an effect on the performance of the equalized signal. The results in Fig. 4.14 indicate that the penalty when using 75% and 50% of the maximum number of taps is approximately similar to the one when using the maximum number of taps. Table. 4.7 shows the OSNR penalty when using the maximum number of taps, also for 75% and 50% of the maximum number of taps to have a BER of 10^{-3}.
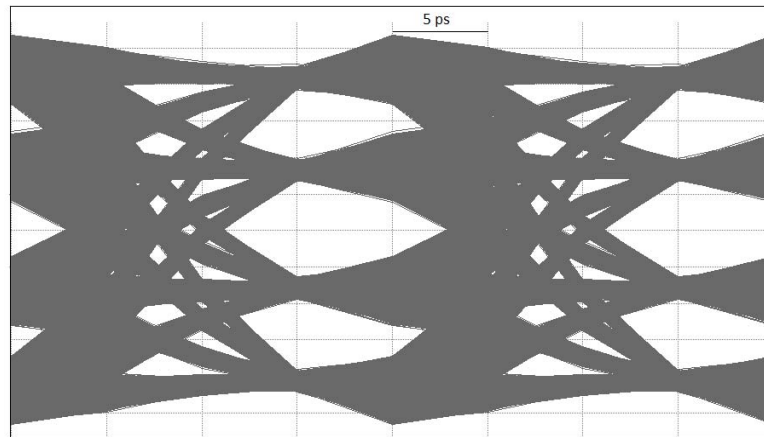
(a)
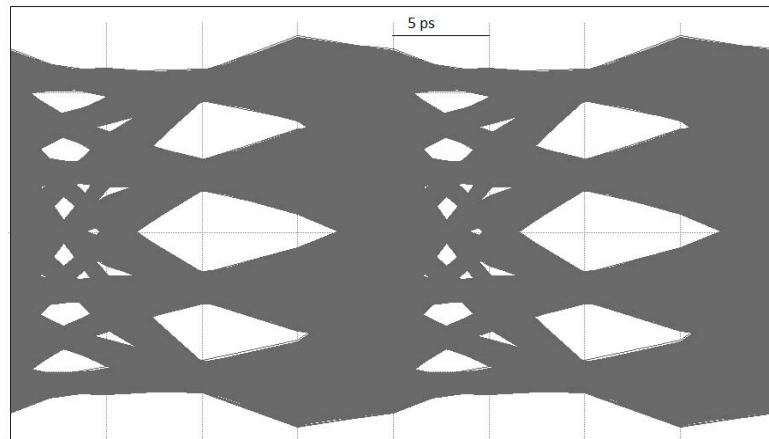
(b)

Figure 4.12: Eye diagrams after CD equalization for distances: 500 km (a) and 1000 km using 4 samples/symbol.

The results indicate that using the maximum number of taps results in OSNR penalty of 0.2 and 0.7 dB for 500 and 1000 km, respectively. While make a reduction in the number of taps to 75% and 50% of the maximum number of taps has a better performance results.

When comparing CD equalization using 2 and 4 samples/symbol, we can notice that using 4 samples gives better results than using 2 samples. In addition, when we reduce the number of taps in terms of 4 samples/symbol to 50% of the maximum number (which is approximately twice the maximum number of taps using 2 samples), it gives better results in terms of OSNR penalty. This indicates that for CD equalization in 400 Gb/s PM-16QAM, using 4 samples/symbol is the best approach to compensate for CD.
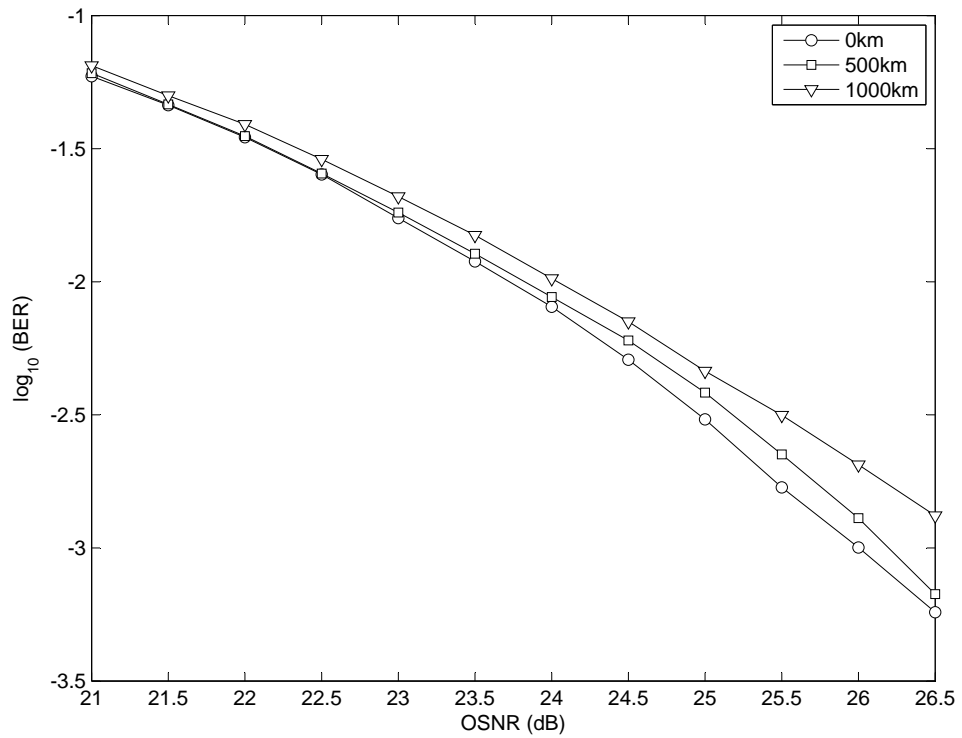
Figure 4.13: BER versus OSNR for 16-QAM using 4 samples/symbol with maximum number of taps.

Distance (km)	OSNR penalty (dB) using N_{max}	OSNR penalty (dB) using 75% of N_{max}	OSNR penalty (dB) using 50% of N_{max}
500	0.2	0.18	0.18
1000	0.7	1.0	0.65

Table 4.7: OSNR penalty of equalized 16-QAM signal using 4 samples/symbol with maximum number of taps, 75% and 50 % of the maximum number of taps at BER of 10^{-3}.
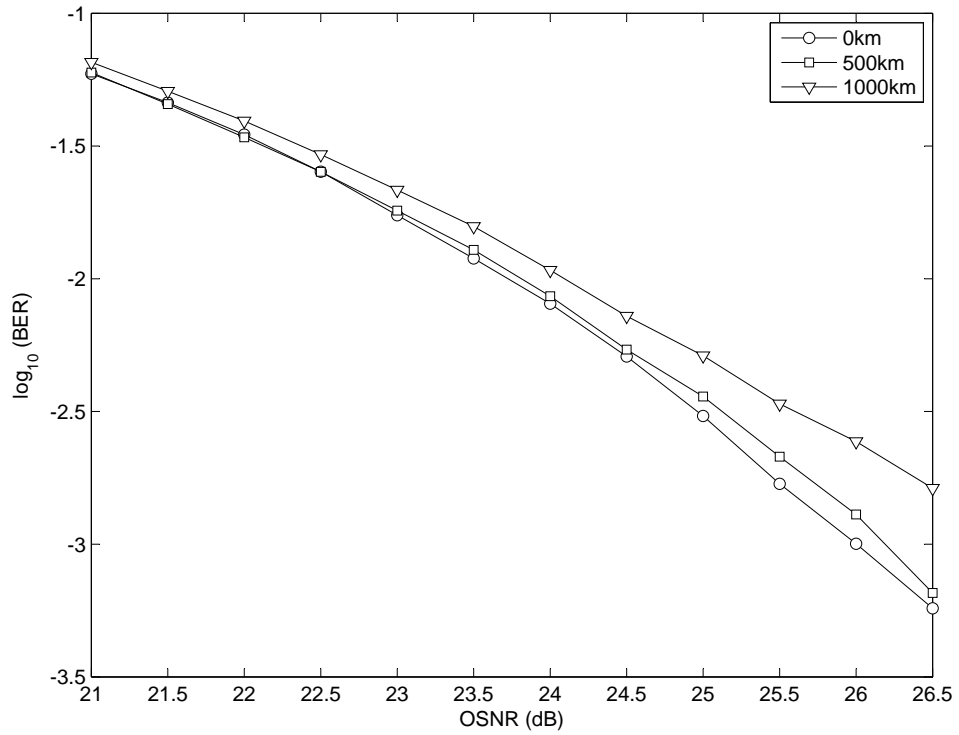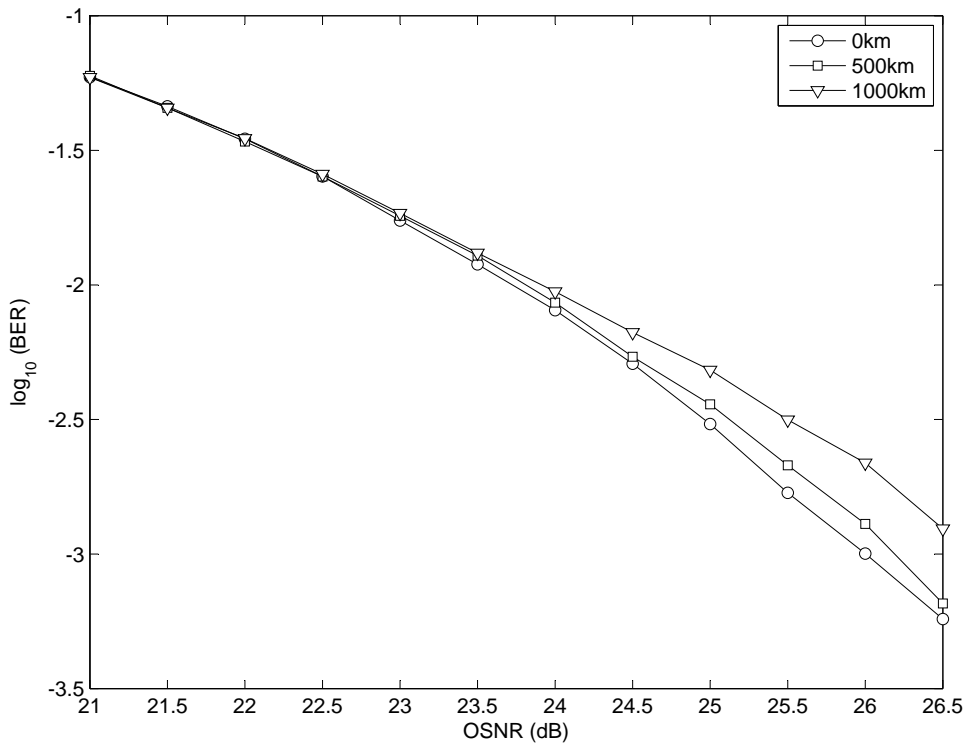
Figure 4.14: BER versus OSNR for 16-QAM using 4 samples/symbol with (a) 75% (b) 50% of the maximum number of taps.

4.6 Maximum Tolerable Fiber Distance for CD Compensating Filter

In previous sections, we have compensated for a static amount of CD using FD-FIR filter. The CD compensating filter was designed to compensate for CD after specific distance, where the number of taps for FD-FIR filter is a function of fiber distance. Since the fiber length may varies (with ± small distance) from the distance that is used to design the CD compensating filter, we tried to calculate the maximum tolerable distance that may not affect the performance after compensating for CD.

We calculate the maximum tolerable distance for 100 Gb/s PM-QPSK and 400 Gb/s PM-16QAM systems using the method presented in [42], where eye closure penalty has been evaluated using computer simulation for different modulation formats. The modulation techniques discussed in [42] are: OOK, BPSK and frequency shift keying (FSK). The simulation results indicate that the system performance depends on the product of $R_s^2 LD$, where R_s is the symbol rate, L is the fiber length and D is the fiber dispersion coefficient.

We calculate ECP to evaluate the penalty due to CD for QPSK and 16-QAM modulation formats and the results are shown in Table. 4.8 for $D = 17$ ps/nm.km . For 100 Gb/s PM-QPSK system with a symbol rate of 25 GSymbol/s, $R_s^2 L$ is found to be 1250 (GSymbol/s)^2 km and the maximum distance is 2 km at 1-dB penalty. While for 400 Gb/s PM-16QAM system with a symbol rate of 50 GSymbol/s, $R_s^2 L$ is found to be 500 (GSymbol/s)^2 km and the maximum distance is 0.2 km at 1-dB penalty. The results for 2-dB penalty are also shown in Table. 4.8.

Modulation format	Maximum tolerable fiber length with D = 17 ps/nm.km	
	@ 1-dB ECP	@ 2-dB ECP
100 Gb/s QPSK	2 km	3.2 km
400 Gb/s 16-QAM	0.2 km	0.38 km

Table 4.8: Maximum tolerable fiber length with D = 17 ps/nm.km at specific ECP for QPSK and 16-QAM modulation formats.

To confirm our finding for 100 Gb/s system, we designed a FD-FIR filter for 1000

km, then we used this filter to compensate for CD with fiber lengths of 1000 km, 1005 km and 1008 km. We generated BER versus OSNR curve for back-to-back (0 km) and with these distances as shown in Fig. 4.15.

From the figure, we notice that with fiber length 1005 and 1008 km there is a notable penalty. The OSNR penalty with 1005 km fiber is about 0.6 dB, while it has higher penalty with 1008 km fiber. The results indicate that a fiber with additional distance more than 8 km will cause a severe performance degradation.

For 400 Gb/s system, we designed a FD-FIR filter for 500 km, then we used this filter to compensate for CD with fiber lengths of 500 km, 501 km and 502 km. We generate BER versus OSNR curve for back-to-back (0 km) and with these distances as shown in Fig. 4.16.

From the figure, we can notice that fiber length 501 and 502 km have severe effect on the performance. The OSNR penalty with 501 km fiber is about 1.7 dB, while it has higher penalty with 502 km fiber. The results indicate that a fiber with additional
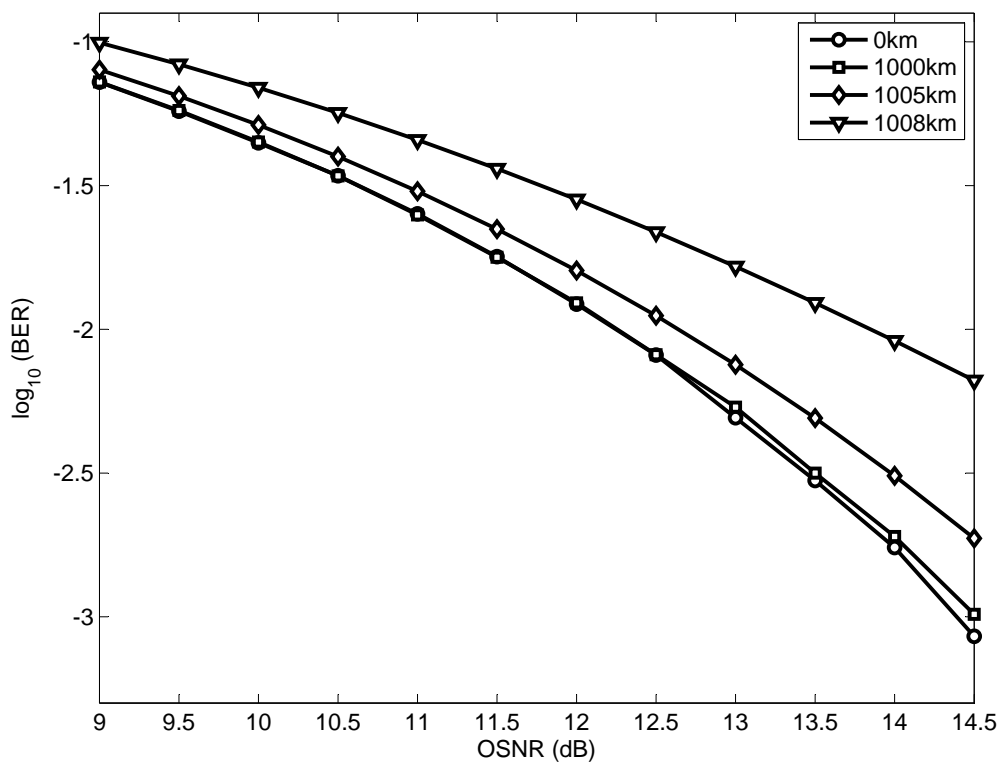
Figure 4.15: BER versus OSNR for 100 Gb/s system with FD-FIR designed for 1000 km with fiber length of 1000, 1005 and 1008 km.
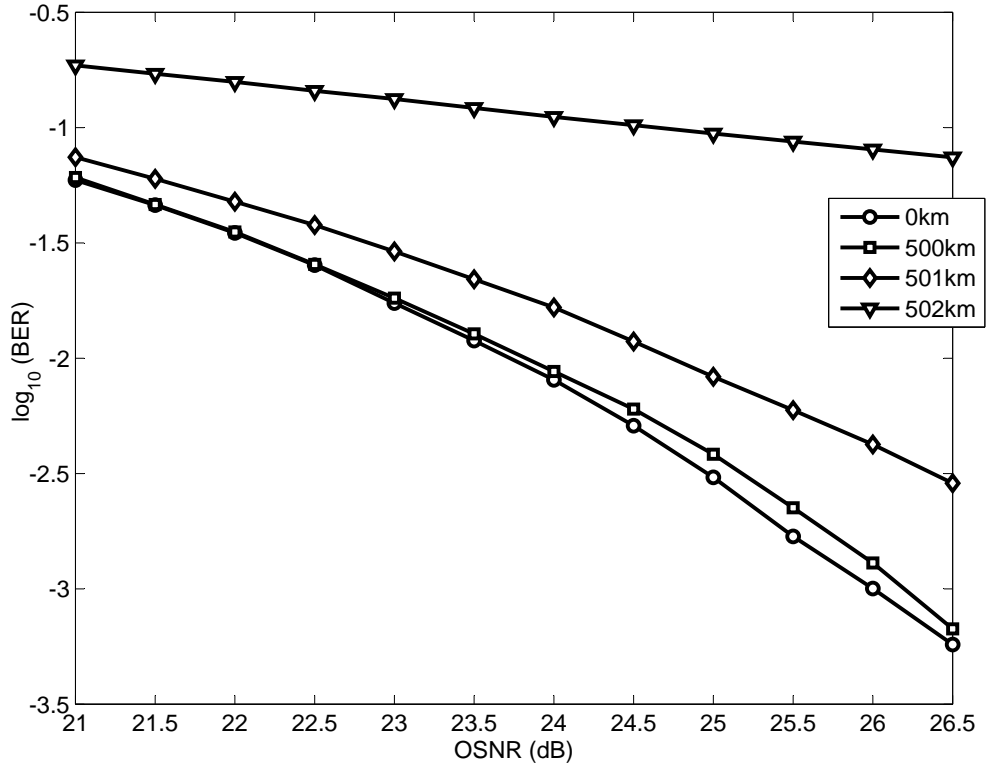
Figure 4.16: BER versus OSNR for 400 Gb/s system with FD-FIR designed for 500 km with fiber length of 501 and 502 km.

distance of 2 km will cause a severe performance degradation. The reason to have such high degradation associated with additional 1 or 2 km is that the system performance of these modulation formats depends on the product of $R_s^2 LD$ that was partially explained in Table. 4.8 and [42]. Also, FD-FIR filter doesn't ideally compensate for CD.

Chapter 5

Conclusions

5.1 Conclusions

The channel data rates of 10 Gb/s and 40 Gb/s will be upgraded in the near future to 100 Gb/s and 400 Gb/s with 50 and 100 GHz channel spacing respectively to match the increase of traffic demands in the recent years. 100 Gb/s systems are already in commercial products, while 400 Gb/s systems are still in research labs.

In this thesis, we use computer simulation to show that cascading filters has a significant impact on high-speed optical transmission systems running at 100 Gb/s and 400 Gb/s for single-carrier and dual-carrier. The results indicate that amplitude and dispersion associated with filter cascades put a limitation on the number of OADM nodes that the WDM signal can pass through in a typical WDM link.

The results of single-carrier system is better than the one of dual-carrier system in terms of ECP and the number of filters that the WDM signal can pass through. This is because in dual-carrier system, both carriers are shifted from the filter's center frequency and there is a crosstalk effect between the two carriers.

Additionally, we have proposed to compensate for linear CD electronically using FD-FIR filter for both 100 and 400 Gb/s systems. We used different sample rates for each system and comparde the results of them. For 100 Gb/s PM-QPSK, the results show that there is no notable OSNR penalty when using 2 and 4 samples/symbol with the maximum number of taps. This indicates that for CD equalization in 100 Gb/s

PM-QPSK, using 2 samples/symbol is the best approach to compensate for CD.

For 400 Gb/s PM-16QAM, the results show that using 4 samples gives better results than using 2 samples. In addition, when we reduced the number of taps in terms of 4 samples/symbol to 50% of the maximum number, it gives better results in term of OSNR penalty compared with the results of using 2 samples/symbol with maximum number of taps. This indicates that for CD equalization in 400 Gb/s PM-16QAM, using 4 samples/symbol is the best approach to compensate for CD.

5.2   Suggestions for Future Work

In CD compensation, we compensated for CD without any consideration for PMD and fiber non-linear effects. Future work should incorporate CD compensation as well as PMD and fiber non-linear effects for 100 Gb/s PM-QPSK and 400 Gb/s PM-16QAM coherent communication systems.

Moreover, we compensated for a static amount of CD using FD-FIR filter without any consideration for a residual CD that may exist. Future work should take into account the residual CD that may exist which can be compensated using adaptive filters (FIR based LMS or FIR based CMA) after compensating for CD using FD-FIR filter. Also, we propose to incorporate the filter cascade with fiber effects (CD and PMD) and study the impact of these factors together and build a DSP model that may compensate for these effects.

References

[1] J. Gowar, Optical communication systems (2nd Edition), Prentice Hall, 1993, Chap.1 & Chap.2.

[2] G. Keiser, Optical fiber communications (2nd Edition), McGraw-Hill Companies, Inc., 1991, Chap. 1.

[3] A. Ghatak and K. Thyagarajan, An introduction to fiber optics, Cambridge University Press, 1998.

[4] Yamamoto, Y.; , "Receiver performance evaluation of various digital optical modulation-demodulation systems in the 0.5-10 m wavelength region," Quantum Electronics, IEEE Journal of , vol.16, no.11, pp. 1251- 1259, Nov 1980.

[5] K. Kikuchi, "Digital coherent optical communications system: fundamental and future prospects, " IEICE Electronics Express, Vol8, No.20, 1642-1662, 2011.

[6] K. Kikuchi, "Coherent optical communications: historical perspectives and future directions," in High Spectral Density Optical Communication Technology, M. Nakazawa, K. Kikuchi, and T. Miyazaki, eds (Springer, 2010), Chap. 2.

[7] G. Keiser, Optical Fiber Communications, 2nd ed. New York: McGraw-Hill, 1991.

[8] `http://www.om.tu-harburg.de/Forschung/Pmd/`

[9] R. Ramaswami and K. Sivarajan, Optical Networks: A Practical Perspective. San Mateo, CA: Morgan Kaufmann, 1998.

[10] Bulow, H.; , "PMD mitigation techniques and their effectiveness in installed fiber," Optical Fiber Communication Conference, 2000 , vol.3, no., pp.110-112 vol.3, 2000

[11] Chapter 14. Finite Impulse Response (FIR) Filters. Dr. Naim Dahnoun, Bristol University, (c) Texas Instruments 2004.

[12] Abd El-Naser; A. Mohammed; Mohamed M. E. El-Halawany; Ahmed Nabih Zaki Rashed; and Mohamoud M. Eid, Optical Add Drop Multiplexers with UW-DWDM Technique in Metro Optical Access Communication Networks ;International Journal of Computer Science and Telecommunications (IJCST), Vol. 2, No. 2, pp. 5-13, April 2011.

[13] Matthew Mitchell, John McNicol, Vinayak Dangui, Han Sun, Kuang-Tsan Wu, Zhong Pan, Michael Van Leeuwen, Jeffrey Rahn, Stephen Grubb, Radhakrishnan Nagarajan, David Welch, Optical integration and multi-carrier solutions for 100G and beyond, Optical Fiber Technology, Volume 17, Issue 5, October 2011, Pages 412-420.

[14] Xia, T.J.; Gringeri, S.; Tomizawa, M.; , "High-capacity optical transport networks," Communications Magazine, IEEE , vol.50, no.11, pp.170-178, November 2012.

[15] J. Michael Harris, Robert Lindquist, JuneKoo Rhee, James E. Webb, "Liquid-Crystal Based Optical Switching," Optical Switching book, Springer, pages. 141-167, 2006.

[16] B. P. Keyworth, " ROADM Subsystems and Technologies," in Optical Fiber Communication Conference and Exposition and The National Fiber Optic Engineers Conference, Technical Digest (CD) (Optical Society of America, 2005), paper OWB5.

[17] C.F.G. Alegria, "All-fibre Devices for WDM Optical Communications", Doct. thesis (University of Southampton, Faculty of Engineering and Science, Department of Electronics and Computer Science, 2001).

[18] http://www.oplink.com/

[19] John Downie, Frank Annunziata, Jason Hurley, and Jaymin Amin, "Fixed low-channel-count optical add-drop multiplexer filter concatenation experiments with 50-GHz channel spacing and 10-Gbit/s NRZ signals," J. Opt. Netw. 3, 204-213 (2004).

[20] http://www.auxora.com/doce/technical-default.html

[21] Khrais, N.N.; Elrefaie, A.F.; Wagner, R.E.; , "Performance degradations of WDM systems due to laser and optical filter misalignments," Electronics Letters , vol.31, no.14, pp.1179-1180, 6 Jul 1995.

[22] Khrais, N.N.; Elrefaie, A.F.; Wagner, R.E.; Ahmed, S.; , "Performance degradation of multi wavelength optical networks due to laser and (de)multiplexer misalignments," Photonics Technology Letters, IEEE , vol.7, no.11, pp.1348-1350, Nov. 1995.

[23] Khrais, N.N.; Elrefaie, A.F.; Wagner, R.E.; Ahmed, S.; , "Performance of cascaded misaligned optical (de)multiplexers in multiwavelength optical networks," Photonics Technology Letters, IEEE , vol.8, no.8, pp.1073-1075, Aug. 1996.

[24] Kuznetsov, M.; Froberg, N.M.; Henion, S.R.; Rauschenbach, K.A. , "Power penalty for optical signals due to dispersion slope in WDM filter cascades," Photonics Technology Letters, IEEE , vol.11, no.11, pp.1411-1413, Nov. 1999.

[25] M. Kuznetsov, N. M. Froberg, S. R. Henion, C. Reinke, C. Fennelly, K. A. Rauschenbach, and R. I. MacDonald, "Dispersion-Induced Power Penalty in Fiber-Bragg-Grating WDM Filter Cascades," in Optical Fiber Communication Conference, OSA Technical Digest Series (Optical Society of America, 2000), paper WM34.

[26] Kuznetsov, M.; Froberg, N.M.; Henlon, S.R.; Reinke, C.; Fennelly, C.; , "Dispersion-induced power penalty in fiber-Bragg-grating WDM filter cascades using optically preamplified and nonpreamplified receivers," Photonics Technology Letters, IEEE , vol.12, no.10, pp.1406-1408, Oct. 2000.

[27] Haiqing Wei, Hwan J. Jeong, Aly F. Elrefaie and David V. Plant, "Dispersion-induced signal distortion in cascaded OADMs", Proc. SPIE 4989, 93 (2003).

[28] Bo Zhang; Malouin, C.; Liu, S.; Schmidt, T.J.; Guangxun Liao; Ping Wang; Washburn, H.; Jim Yuan; , "Penalty-free transmission of 127-Gb/s coherent PM-QPSK over 1500-km of NDSF with 10 cascaded 50-GHz ROADMs," Optical Fiber Communication (OFC), collocated National Fiber Optic Engineers Conference, 2010 Conference on (OFC/NFOEC) , vol., no., pp.1-3, 21-25 March 2010.

[29] A. H. Gnauck, P. J. Winzer, S. Chandrasekhar, X. Liu, B. Zhu, and D. W. Peckham, "Spectrally Efficient Long-Haul WDM Transmission Using 224-Gb/s Polarization-Multiplexed 16-QAM," J. Lightwave Technol. 29, 373-377 (2011).

[30] Nelson, L.E.; Woodward, S.L.; Foo, S.; Moyer, M.; Yao, D.; O'Sullivan, M.; , "100Gb/s dual-carrier DP-QPSK performance after WDM transmission including 50GHz wavelength selective switches," Optical Fiber Communication Conference and Exposition (OFC/NFOEC), 2011 and the National Fiber Optic Engineers Conference , vol., no., pp.1-3, 6-10 March 2011.

[31] V. Sleiffer, D. van den Borne, V. Veljanovski, M. Kuschnerov, M. Hirano, Y. Yamamoto, T. Sasaki, S. L. Jansen, and H. Waardt, de, "Transmission of 448-Gb/s dual-carrier POLMUX-16QAM over 1230 km with 5 flexi-grid ROADM passes," in Optical Fiber Communication Conference, OSA Technical Digest (Optical Society of America, 2012), paper OW4C.3.

[32] A. Färbert, S. Langenbach, N. Stojanovic, C. Dorschky, T. Kupfer, C. Schulien, J. P. Elbers, H. Wernz, H. Griesser, and C. Glingener, Performance of a 10.7 Gb/s

receiver with digital equaliser using maximum likelihood sequence estimation, in Proceeding of IEEE European Conference on Optical Communication, 2004.

[33] S. Tsukamoto; K. Katoh; K. Kikuchi; , "Unrepeated transmission of 20-Gb/s optical quadrature phase-shift-keying signal over 200-km standard single-mode fiber based on digital processing of homodyne-detected signal for Group-velocity dispersion compensation," Photonics Technology Letters, IEEE , vol.18, no.9, pp.1016-1018, May 1, 2006.

[34] Savory, S.J.; Gavioli, G.; Killey, R.I.; Bayvel, P.; , "Transmission of 42.8Gbit/s Polarization Multiplexed NRZ-QPSK over 6400km of Standard Fiber with no Optical Dispersion Compensation," Optical Fiber Communication and the National Fiber Optic Engineers Conference, 2007. OFC/NFOEC 2007. Conference on , vol., no., pp.1-3, 25-29 March 2007.

[35] Seb J. Savory, Giancarlo Gavioli, Robert I. Killey, and Polina Bayvel, "Electronic compensation of chromatic dispersion using a digital coherent receiver," Opt. Express 15, 2120-2126 (2007).

[36] Seb J. Savory, "Digital filters for coherent optical receivers," Opt. Express 16, 804-817 (2008).

[37] Savory, S. J.; , "Compensation of fibre impairments in digital coherent systems," Optical Communication, 2008. ECOC 2008. 34th European Conference on , vol., no., pp.1-4, 21-25 Sept. 2008.

[38] Savory, S.J.; , "Digital Coherent Optical Receivers: Algorithms and Subsystems," Selected Topics in Quantum Electronics, IEEE Journal of , vol.16, no.5, pp.1164-1179, Sept.-Oct. 2010.

[39] Tianhua Xu, Gunnar Jacobsen, Sergei Popov, Jie Li, Evgeny Vanin, Ke Wang, Ari T. Friberg, and Yimo Zhang, "Chromatic dispersion compensation in coherent transmission system using digital filters," Opt. Express 18, 16243-16257 (2010).

[40] Tianhua Xu, Gunnar Jacobsen, Sergei Popov, Jie Li, Ke Wang and Ari T. Friberg, "Digital compensation of chromatic dispersion in 112-Gbit/s PDM-QPSK system", Proc. SPIE 7632, 763202 (2009).

[41] Goldfarb, G.; Guifang Li; , "Chromatic Dispersion Compensation Using Digital IIR Filtering With Coherent Detection," Photonics Technology Letters, IEEE , vol.19, no.13, pp.969-971, July1, 2007.

[42] A. F. Elrefaie, R. E. Wagner, D. A. Atlas, and D. G. Daut, Chromatic dispersion limitations in coherent lightwave transmission systems, J. Lightwave Technol., vol. 6, pp. 704709, May 1988.

[43] G. P. Agrawal, Fiber-Optic Communication Systems, 4th edition(Wiley, 2010).

[44] Roberts, K.; Beckett, D.; Boertjes, D.; Berthold, J.; Laperle, C.; , "100G and beyond with digital coherent signal processing," Communications Magazine, IEEE , vol.48, no.7, pp.62-69, July 2010.

[45] http://www.vpisystems.com/.

[46] http://www.tek.com/.

Vita

Rami Yousef Al-Dalky was born on December 7, 1986, in Irbid, Jordan. He was educated in local public schools and graduated from Irbid High School, Jordan, in 2004.

He received his Bachelor of Science degree in Computer Engineering from Jordan University of Science and Technology (JUST) in 2009.

Mr. Al-Dalky worked in Cisco TAC then in Central Bank of Jordan as IT Engineer. In 2011, he joined American University of Sharjah (AUS) to pursue his M.S degree, and granted the graduate teaching assistantship from there. He was awarded the Master of Science degree in Computer Engineering in 2013. Mr. Al-Dalky is a member of Jordanian Engineers Association.